

Landslides (2021) 18:281–302
 DOI 10.1007/s10346-020-01444-0
 Received: 1 September 2019
 Accepted: 28 May 2020
 Published online: 30 June 2020
 © Springer-Verlag GmbH Germany
 part of Springer Nature 2020

Ye Hua · Xianmin Wang · Yongwei Li · Peiyun Xu · Wenxiang Xia

Dynamic development of landslide susceptibility based on slope unit and deep neural networks

Abstract The Three Gorges Reservoir is one of the areas with the most serious landslide hazards in China. Landslide susceptibility indicates where landslides are prone to occur in the future under the influences of certain geoenvironmental and triggering conditions and is an important way for landslide prevention. This work employs multi-source and three-temporal landslide monitoring data (geology, terrain, hydrology, and remote sensing data) to reveal the dynamic change of landslide susceptibility with time in the Badong-Zigui section in the Three Gorges area. Nine influence factors for landslides (land use, aspect, engineering rock group (ERG), slope, distance to river (DTR), relative relief, normalized difference water index (NDWI), normalized difference vegetation index (NDVI) and annual cumulative rainfall (ACR)) are generated from the monitoring data. The algorithms of slope unit segmentation and deep neural networks are adopted to conduct landslide susceptibility evaluations in the 3 years of 2002, 2007, and 2017 and to investigate the dynamic change of landslide susceptibility. Moreover, this work also reveals the dynamic response of landslide susceptibility to the changing factors of rainfall, reservoir water fluctuation, soil moisture, and land use. Some new viewpoints are suggested as follows. (1) The main factors affecting landslide occurrence are DTR, NDWI, relative relief, and ERG. Among them, DTR contributes most in all the 3 years; thus, reservoir water fluctuation has the most important impact on landslide occurrence in the study area. (2) From 2002 to 2007, the new high-susceptibility areas mainly appeared along the Yangtze River and also distributed around the roads. From 2007 to 2017, more than half of the new high-susceptibility areas were distributed around the roads, and susceptibility increases also occurred in the mountainous areas far from the Yangtze River. (3) The development of landslide susceptibility from 2002 to 2007 was mainly caused by the rising of reservoir water level as well as road construction. The change of landslide susceptibility from 2007 to 2017 was mainly caused by rainfall and road construction. This work may provide some clues on landslide prevention and control according to the dynamic development of landslide susceptibility and the causes of the susceptibility changes.

Keywords Slope unit · Landslide susceptibility · Deep neural networks · The Three Gorges Reservoir

Introduction

The Three Gorges Reservoir area, characterized by steep terrain, impounded reservoir, and abundant rainfall (Zhe et al. 2013), has long been a high-risk area for landslide disasters (Liang et al. 2016). According to the statistics from the Three Gorges Reservoir Area Geological Disaster Prevention and Control Work Command (TGWC), more than 4600 landslides and collapses have occurred in the reservoir area. Thus, it is urgent and necessary to take preventive measures for landslide disasters there. Landslide susceptibility evaluation (LSE) is an effective means to determine the

areas most prone to landslides and to discover the key regions for landslide prevention and control (Brabb 1987; Guzzetti et al. 2006; Fell et al. 2007); thus, it is an important technique and means to prevent landslides (Fell et al. 2007; Guzzetti et al. 2012). The objective of this work is to conduct LSE and to reveal the rules and causes of the dynamic development of landslide susceptibility in the Badong-Zigui section in the Three Gorges area.

For large areas lacking in proper and detailed geotechnical information, statistical-based methods were commonly used to conduct landslide susceptibility analysis (Cascini 2008; van Westen et al. 2008; Guzzetti et al. 2012). The present researches on LSE mainly employed the following methods. (1) Traditional regression analysis methods, e.g., frequency ratio (e.g., Youssef et al. 2014; Li et al. 2017; Mandal et al. 2018; Lee et al. 2015), index of entropy models (e.g., Youssef et al. 2014; Wang et al. 2016b; Mondal and Mandal 2019), landslide density (e.g., Barella et al. 2019; Sharir et al. 2017), logistical regression (LR) (e.g., Martinović et al. 2016; Tanyas et al. 2019; Nefeslioglu and Gorum 2020), weights of evidence (e.g., Pamela and Yukni 2017; Bacha et al. 2018; Hong et al. 2017; Wang et al. 2016a), and fisher discriminant analysis (FDA) (e.g., Gupta et al. 2018; Wang et al. 2020a; He et al. 2012; Binh and Prakash 2019). Tanyas et al. (2019) investigated 64 earthquake-induced landslide (EQIL) inventories and adopted logistical regression and slope unit to conduct LSEs in 25 EQIL areas. The model reached the area under curve (AUC) precision of 0.88 when applied in the Wenchuan event, one example of the EQIL study areas. Nefeslioglu and Gorum (2020) revealed the landslide hazards and suggested the use of landslide hazard maps in determining mitigation priorities in the Melen Dam reservoir and its protection area. Logistic regression analysis was employed to conduct LSE and achieved a good result of landslide spatial probability. Gupta et al. (2018) used information value method to calculate the weights of various influence factors and applied the weights into the methods of FDA and binary LR to conduct LSEs. Moreover, the method of Heidke-Skill-Score was employed to assess the prediction accuracy, and the scores of FDA and LR are 0.89 and 0.90, respectively. Barella et al. (2019) compared seven statistical methods for LSE including landslide density, likelihood ratio, information value, Bayesian model, weights of evidence, logistic regression, and discriminant analysis, and the method weights of evidence outperformed the other methods in the evaluation accuracy. Traditional regression analysis methods generally employ a landslide inventory as the predictive variable and establish statistical regression models to predict the probability of landslide occurrence. However, there is a certain degree of subjectivity in factor selection and weight (or other parameters) assignment, so this kind of methods, to some degree, rely on expert experience (Kanungo et al. 2011; Gupta et al. 2018). (2) Traditional machine learning methods and the ensemble techniques, e.g., artificial neural network (ANN) (e.g., Gorsevski et al. 2016; Wei et al.

2017; Sevgen et al. 2019; Polykretis and Chalkias 2018), random forest (RF) (e.g., Sevgen et al. 2019; Kim et al. 2018; Zhang et al. 2017; Shirvani 2020), support vector machine (SVM) (e.g., Dieu et al. 2019; Wu et al. 2016; Pham et al. 2019; Yu et al. 2019; Kumar et al. 2017), Classification and Regression Treebagger (ClaReT) (e.g., Lagomarsino et al. 2017), and genetic algorithm (GA)-SVM (e.g., Niu et al. 2017; Ramachandra et al. 2013). Binh et al. (2019) utilized four different ensemble techniques for landslide susceptibility assessment and prediction, including bagging-based reduced error pruning trees (BREPT), multiboost-based reduced error pruning trees (MBREPT), rotation forest-based reduced error pruning trees (RFREPT), and random subspace-based reduced error pruning trees (RSREPT). BREPT and RFREPT performed better than the other two methods, and the four ensemble methods all prevailed over the method of reduced error pruning trees (REPT). Dou et al. (2020) implemented LSE by using the four methods of SVM-Stacking, SVM, SVM-Bagging, and SVM-Boosting. The SVM-boosting model outperformed the other three models, while the SVM-Stacking model had the poorest performance. Zhao and Chen (2020) utilized ensemble techniques for landslide susceptibility modeling, including functional trees (FT), bagging-functional trees (BFT), rotation forest-functional trees (RFRT), and dagging-functional trees (DFT), and BFT surpasses the other methods in the AUC precision of 0.804. Dieu et al. (2019) employed a classifier of support vector machine (SVM), and four meta/ensemble techniques including Adaboost (AB), bagging (BA), rotation forest (RF), and random subspace (RS) to construct new ensemble models and to implement LSEs. RS_SVM is superior to the methods of SVM, RF_SVM, BA_SVM, and AB_SVM in the prediction accuracy. Traditional machine learning methods possess an important common on selection of various critical influence factors, which can reduce the impact of highly correlated factors on the generalization capability of the models (Bui et al. 2016). Moreover, these methods can support the comprehensive analysis of multiple influence factors and relatively well depict the nonlinear correlation between the influence factors and landslide susceptibility; thus, they can achieve relatively high LSE precisions (Huang and Zhao 2018; Bui et al. 2016).

(3) Deep learning methods. There appear some, but still relatively few, works implementing LSEs by deep learning. Fang et al. (2020) integrated convolutional neural network (CNN) with three traditional classifiers of support vector machine (SVM), random forest (RF), and logistic regression (LR) to assess landslide susceptibility. The integration of CNN with SVM, RF, or LR can effectively improve the performances of the three traditional classifiers (Fang et al. 2020). Wang et al. (2020b) adopted recurrent neural networks (RNNs) to perform landslide susceptibility mapping in Yongxin County, China, and proposed that the RNN framework was useful for landslide susceptibility mapping to mitigate and manage landslides. Wang et al. (2019a) utilized a CNN framework for landslide susceptibility mapping in Yanshan County, China, and indicated that CNN performed well for landslide prevention and management. Dong et al. (2020) implemented LSE by using a spatially explicit deep learning neural network model, and several performance metrics showed that the model performed well for landslide evaluation and prediction both in training precisions (AUC = 0.90, accuracy = 82%, and RMSE = 0.36) and in predicting future landslides (AUC = 0.89, accuracy = 82%, and RMSE = 0.38). Compared with traditional

machine learning methods, deep learning possesses more complicated structures (Ronoud and Asadi 2019) and thus is more competitive in depicting a complex nonlinear problem (Cao et al. 2019a), such as a landslide system. Moreover, deep learning may achieve better generalization abilities than traditional machine learning due to the capable study strategy (Liu et al. 2019; Duo et al. 2019). It still needs to be illuminated that the LSE precision of a method is highly region-dependent, and the precision of a method may vary largely when it is applied to different areas (Lagomarsino et al. 2017).

Great progresses have been achieved in the LSE studies; however, there are still some limitations for the present researches on LSE. (1) Present studies generally employed traditional regression analysis or traditional machine learning methods to conduct LSE. These methods tend to construct the prediction models with relatively simple structures and to some degree possess the defects in delineating the complicated nonlinear landslide systems and in preventing the overfitting problem. Compared with these methods, deep learning methods, e.g., deep neural networks (DNNs), have prominent advantages to the above problems. Two important features of DNNs are nonlinear and multi-layer structures, so they can well depict a complicated nonlinear landslide system affected by various influence factors. Moreover, valid algorithms such as “Dropout” or “Batch” are included in DNNs to effectively prevent overfitting. Therefore, DNNs are hopeful to improve the evaluation accuracy of landslide susceptibility. However, there are relatively few researches conducting LSE by deep learning methods. (2) Present researches generally evaluated the static landslide susceptibility under a single time point. However, the influence factors for landslide occurrence and development, e.g., water level, rainfall, and human activity, always change with time; thus, landslide susceptibility also correspondingly dynamically changes (Gorsevski et al. 2006; Torizin et al. 2018). Landslide susceptibility changes with time and with the development of the influence factors. Nefeslioglu and Gorum (2020) also proposed that landslide susceptibility maps should be dynamic maps and their regular updating is necessary based on new land-use policies.

Focusing on the above two limitations, this work makes two improvements on landslide susceptibility analysis. (1) Deep neural networks, combined with slope unit segmentation, are employed to obtain a high-precision LSE; (2) Dynamic development of landslide susceptibility is revealed with the changing of the influence factors such as rainfall, human activity, soil moisture, and reservoir water level. The causes of the dynamic change of landslide susceptibility are disclosed including the relation between the change of various influence factors and the development of landslide susceptibility, and the dynamic response of landslide occurrence probability to various changing influence factors.

Focusing on the study area of the Zigui-Badong section in the Three Gorges area, this work employs multi-source and three-temporal landslide monitoring data (geological, topographic, hydrological, and remote sensing data) to investigate landslide susceptibility and its dynamic development. Slope unit segmentation and deep machine learning are adopted to improve the accuracy of LSE. Some new viewpoints on the following three questions are proposed: (1) Which key factors influence landslide susceptibility? (2) What are the development characteristics of landslide susceptibility in the study area? (3) What are the dynamic responses of landslide occurrence probability to various changing factors?

Study area

The study area is located along the Yangtze River from Badong to Zigui Counties in the Three Gorges Reservoir area within 110° 18' E to 110° 49' E longitude and 30° 54' N to 31° 5' N latitude. It covers an area of about 400.77 km² (Fig. 1) and is generally in the shape of a basin. There are two main mountain ranges: Dabie Mountain Range and Wushan Mountain Range, and the elevation varies from ~ 80 to ~ 2000 m. According to the 1:50,000 geological map, the exposed strata in the study area include Quaternary (Q) slopes, metamorphic rocks, and sedimentary rocks. The sedimentary rocks primarily include dolomite, schist, marl, sandstone, and shale (Bai et al. 2010; Ling et al. 2014). The exposure region of metamorphic rocks in the study area is relatively small, and only a small amount of metamorphic rock formations are exposed in the core of the Huangling anticline (MGMR, Ministry of Geology and Mineral Resources 1988; Bai et al. 2009; Wu et al. 2014). Fractures and folds are the main geological structures developed in the study area (MGMR, Ministry of Geology and Mineral Resources 1988; Ehret et al. 2010; Ling et al. 2014). The former mainly includes the Jiuwanxi fault, Xiannvshan fault, Xiangluping fault, and Badong Niukou fault; the main folds were formed in the Zigui syncline, Huangling anticline, Guandukou syncline, and Baifuping anticline (MGMR, Ministry of Geology and Mineral Resources 1988).

The reservoir water level has changed a lot. As the reservoir water level rose from 66 to 135 m, to 156 m, and then to 175 m (Table 1), it has experienced three water storage periods (TGWC, Three Gorges Reservoir Area Geological Disaster Prevention and Control Work Command 2010). In order to ensure the tasks of flood control, water storage, and power generation, the reservoir water level mainly periodically fluctuated between 145 m and 175 m after the completion of the Three Gorges Reservoir in 2009 (according to the statistical data of Three Gorges Geological Disaster Monitoring and Early Warning Center).

The fluctuation has a negative impact on the stability of the bank slopes on both sides of the reservoir area, and provides favorable conditions for landslide occurrences along the Yangtze River. In this work, distance to river (DTR) is adopted as an environmental factor to measure the effect of reservoir water fluctuation, because the change of reservoir water level mainly affects the areas close to the reservoir water.

The rainfall in the study area is abundant. According to the monitoring data from 2002 to 2017 (Fig. 2), the annual cumulative rainfalls in Zigui and Badong were 1196.9 mm and 1082.1 mm, respectively.

Data and methods

Data

Landslide investigation in the study area was conducted by both field survey and Google and Sentinel-2A images. The landslide inventories up to 2007 were obtained via field survey and provided by TGWC. The new landslide inventory in 2017 was interpreted from the Google images and the Sentinel-2A images (Fig. 3). There were 15 newly occurred landslides from 2007 to 2017 with the total increasing area of about 78,157 m². There are two types of landslides in the study area: Quaternary deposit landslides and rock landslides. Among the 238 landslides in the study area, there are 201 Quaternary deposit landslides and 37 rock landslides.

The multi-source monitoring data are listed in Table 2. Five sets of monitoring data are employed to establish the influence factors of landslides and then conduct LSE. (1) DEM data are adopted to build the factors of aspect, slope, and relative relief; (2) Geological map is used to acquire the distribution of engineering rock group (ERG); (3) Hydrological monitoring data are employed to construct the precipitation factor of annual cumulative rainfall (ACR); (4) Remote sensing images are adopted to generate the factors of land use, normalized difference vegetation index (NDVI), normalized difference water index (NDWI), and DTR. In this work, the three-temporal monitoring data include remote sensing images and rainfall data in 2002, 2007, and 2017. Therefore, the dynamic influence factors consist of DTR, land use, NDVI, NDWI, and ACR, which results in the dynamic development of landslide susceptibility. Note the rainfall data were collected from 25 rainfall stations in or around the study area. According to the rainfall values in the 25 stations, the inverse-distance-weighted (IDW) interpolation method is employed to obtain the spatial distribution of rainfall. Moreover, the employed remote sensing images (Landsat 4-5 TM and Landsat 8) are in the resolution of 30 m, so the data of all the influence factors are unified to the same resolution of 30 m. In addition, all the landslides are portrayed with polygons on the 30-m-resolution grid.

There are two reasons why the three years (2002, 2007, and 2017) of monitoring data are selected. (1) In the Three Gorges Reservoir area, the impoundment and fluctuation of reservoir water have important impacts on landslide occurrence. The maximum impounding levels of reservoir water in the 3 years (2002, 2007, and 2017) were 66 m, 156 m, and 175 m, respectively. Thus, in order to reflect the impact of reservoir water level on landslide susceptibility, the 3 years of landslide monitoring data are selected that correspond to the impounding stages of reservoir water. (2) In the study area, land use and road construction also have important influences on landslide occurrence. However, in a short period of time, land uses and roads have changed less, and rare new landslides have occurred in the study area; thus, landslide susceptibility has also less changed. Therefore, according to the above two reasons, the 3 years of monitoring data are selected that have long time intervals and correspond to the impounding stages of reservoir water. Consequently, the dynamic development of landslide susceptibility can be better revealed.

Methods

Figure 4 shows the flowchart of the dynamic LSE in this study. The purpose is to reveal the dynamic development characteristic of landslide susceptibility and its response to various changing factors. First, multi-source monitoring data are employed to extract the monitoring information. Second, nine influence factors are generated in total and include the geoenvironmental and triggering factors, covering almost unchanged and varying factors; Third, LSE is conducted based on slope unit segmentation and DNNs. The study area is segmented into slope units according to the terrain features. Compared with the generally used grid unit, slope unit can better reflect the topography constraints on landslide occurrence and development. Thus, it is hopeful to improve the accuracy of LSE and make LSE more accordant with the actual situation. Then, the LSE model is constructed by DNN algorithm, and LSEs in the 3 years (2002, 2007, and 2017) are conducted by a combination of slope unit and DNN. Fourth, the dynamic

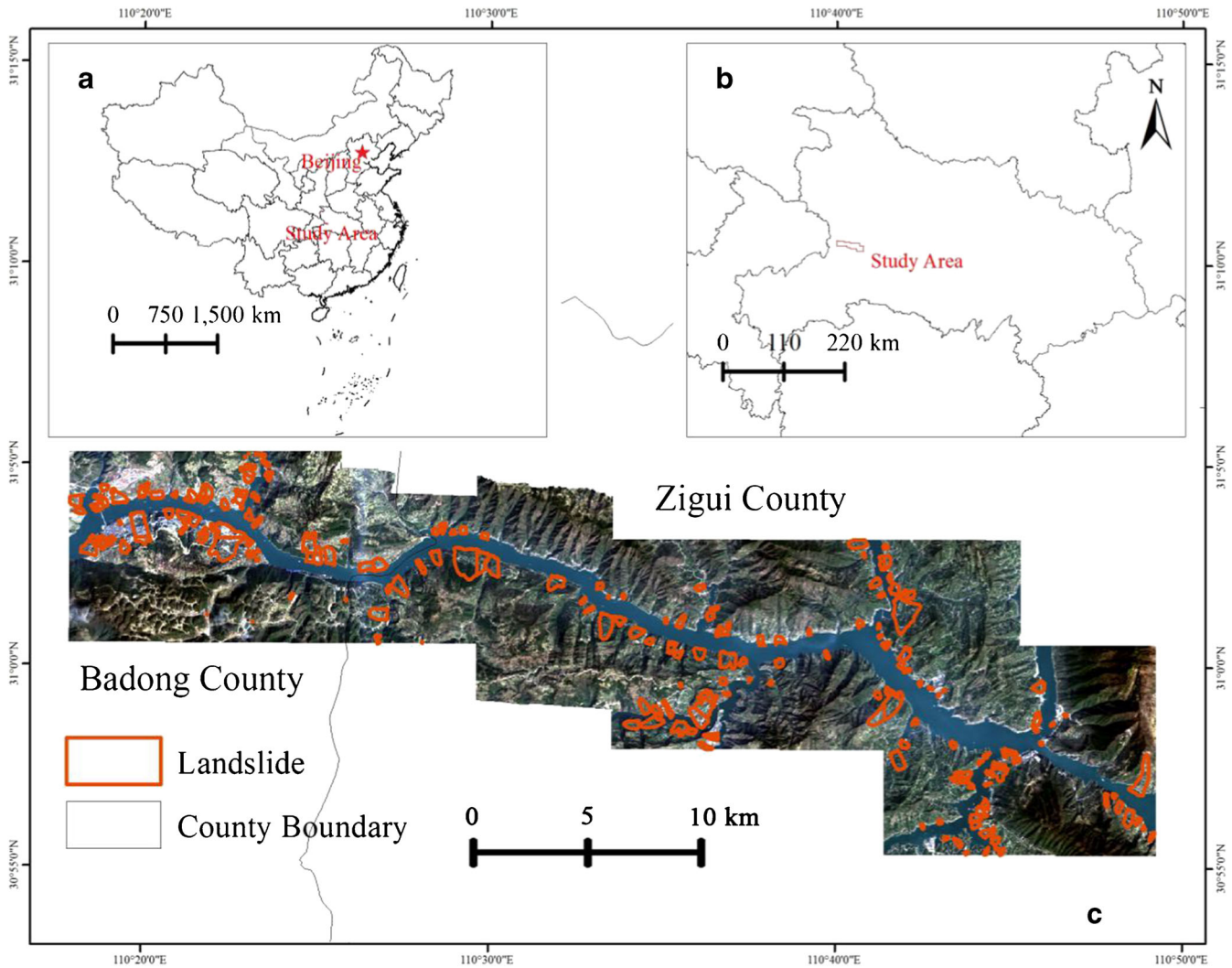


Fig. 1 Location map of the study area and landslide distribution. (a) Location of the study area in China. The base map is sourced from https://download.csdn.net/download/yzy_xiaoyue/10612119. (b) Location of the study area in Hubei Province. The background map is sourced from https://download.csdn.net/download/yzy_xiaoyue/10612119. (c) Landsat 8 image and landslide distribution in the study area. The image was shot in 2017, and the county boundary is sourced from https://download.csdn.net/download/yzy_xiaoyue/10612119

development of landslide susceptibility and the causes of the landslide susceptibility change are revealed. The importance values and contributions of various control and triggering factors to landslides are determined, and then the cause mechanism of landslides in the study area is disclosed. Furthermore, the rule and characteristic of the dynamic development of landslide

susceptibility are revealed. Then, the relation between the development of landslide susceptibility and the change of various influence factors is analyzed to illuminate the dynamic response of landslide occurrence probability to various influence factors.

Geological and environmental factors and triggering factors

Nine influence factors are established from the monitoring data, which are closely related to the local landslide occurrence and development (Fig. 5 and Fig. 6). The nine factors are land use, aspect, ERG, slope, DTR, relative relief, NDWI, NDVI, and ACR. These factors are composed of two types: geological and environmental factors and triggering factors. Geological and environmental factors include slope, aspect, relative relief, ERG, DTR, NDWI, and NDVI. Among these factors, DTR, NDWI, and NDVI have dynamically changed, and the others have kept relatively static. During different years, DTR has varied due to the rising of reservoir water level and the emergence of tributaries. NDWI has

Table 1 Changes of reservoir water level over time (TGWC, Three Gorges Reservoir Area Geological Disaster Prevention and Control Work Command 2010)

Time	Maximum water level (m)
Before 2003.6	66
2003.6–2006.8	135
2006.9–2008.9	156
2009.1–present	175

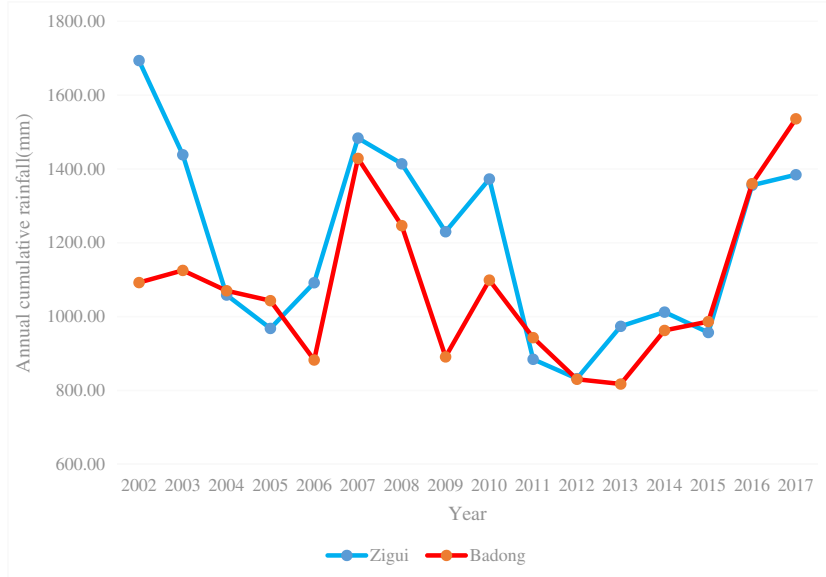


Fig. 2 Variation of the annual cumulative rainfall (ACR) in the study area from 2002 to 2017. The rainfall monitoring data before 2013 are from the Three Gorges Reservoir Area Geological Disaster Prevention and Control Work Command (TGWC), and the rainfall monitoring data after 2013 are from Hubei Provincial Hydrology and Water Resources Bureau (<http://113.57.190.228:8001/web/Report/CantonRainSta>)

changed with rainfall and NDVI has varied with vegetation growth and human activity. Triggering factors consist of rainfall and land use that have dynamically changed with time, and land use actually reflects human activity.

The spatial or spatial-temporal distribution characteristics of various influence factors are revealed. With regard to the static

geological and environmental factors, as shown in Fig. 5, the areas with steeper slopes are mainly distributed in the north and southeast of the study area. Hard rocks mainly appear in the south of the Yangtze River in Badong County and in the eastern part of Zigui County. Soft rocks and soft-hard lithologic groups primarily spread over the remaining regions. Moreover,

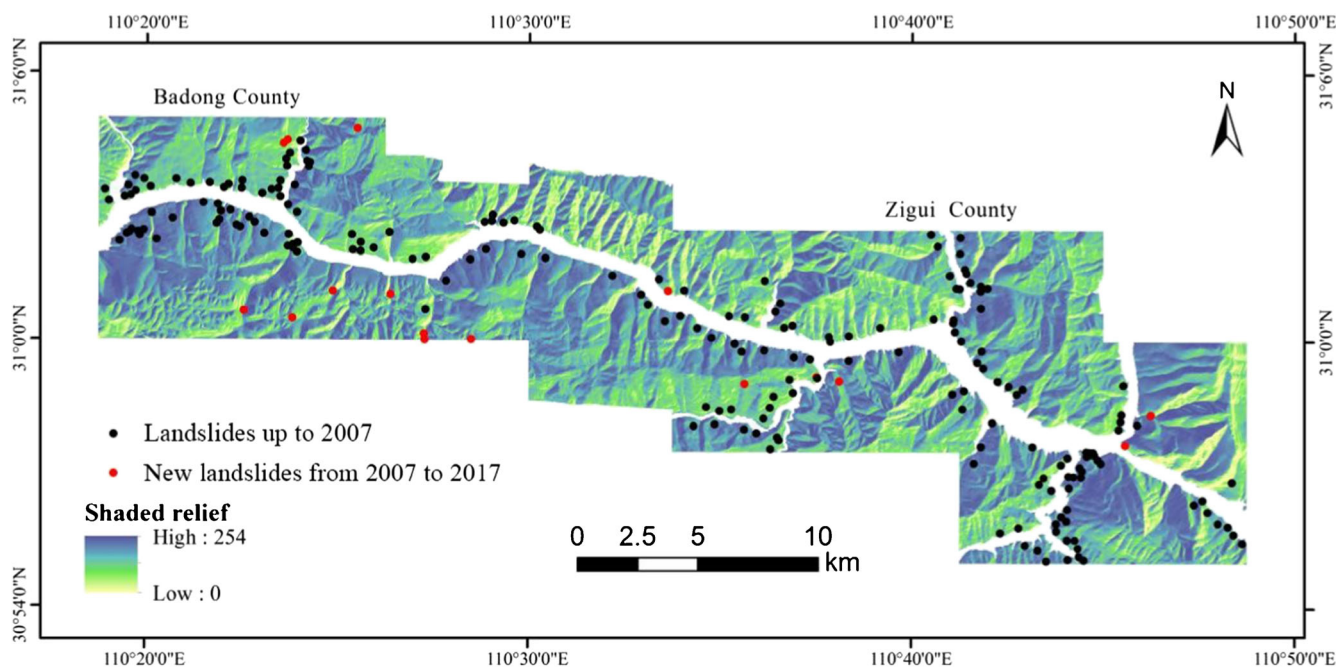


Fig. 3 Landslide investigation in the study area. The new landslides from 2007 to 2017 are interpreted from the Google images and Sentinel-2A images. The Google images were shot on August 27, 2007, April 14, 2015, and October 9, 2017, respectively. The Sentinel-2A images were acquired on December 16, 2015, and July 10, 2017, respectively

Table 2 Multi-source and three-temporal landslide monitoring data and the corresponding influence factors. The meanings of the abbreviations are as follows. DEM: digital elevation model; ERG: engineering rock group; ACR: annual cumulative rainfall; NDVI: normalized difference vegetation index; NDWI: normalized difference water index; DTR: distance to river

Data type	Year/date	Influence factors	Source
DEM (10 m)	2012	Aspect, slope, relative relief	China and Brazil Earth Resource Satellite (CBERS)
Geologic map (1:50000)	2012	ERG	Three Gorges Reservoir Area Geological Disaster Prevention and Control Work Command (TGWC)
Hydrological monitoring data	2002, 2007, 2017	ACR	TGWC Hubei Provincial Hydrology and Water Resources Bureau (HPHWRB)
Landslide investigation	2002, 2007, 2017		TGWC, Google images, Sentinel-2A images
Remote sensing images (30 m)	2002.3, 2007.8, 2017.3	Land use, NDVI, NDWI, DTR	Landsat 4-5 TM, Landsat 8

the eastern part of Zigui County is characterized by relatively high relief.

As for the dynamically changing geological and environmental factors, Fig. 6 (a)–(c) show that tributaries emerged due to the changing of the water level in the Three Gorges reservoir. There was almost one main river in 2002, whereas there had appeared many tributaries till 2017. In 2002, there was nearly no tributary along the Yangtze River in the study area, while by 2007, there had appeared several tributaries. As the reservoir water level continued to rise from 2007 to 2017, the Yangtze River and its tributaries became wider and wider. The area may have been eroded by the cyclical change of the water level, and the erosion degree may have been increased with the appearance of more tributaries. Thus, DTR is a good indicator to describing the impacts of river erosion and reservoir water fluctuation on landslides. As shown in Fig. 6 (d)–(f), the NDVI values in 2002 and 2017 were clearly lower than that in 2007. Besides, in 2017, the NDVI value was slightly higher than in 2002. As depicted in Fig. 6 (g)–(i), the NDWI value in 2017 was significantly higher than in 2002 and 2007, while the NDWI value in 2007 was the lowest. However, in 2007, due to the widening of the river channel, the area where the NDWI values over 0 was more than that in 2002. In addition, the relatively high NDWI values in 2002 and 2007 were mainly concentrated near the bank of the Yangtze River; while in 2017, the

NDWI values of the entire study area were relatively high, except for some mountainous areas.

With respect to the triggering factors, land use associated with human activity is shown in Fig. 6 (j)–(l). From 2002 to 2017, agricultural lands had declined in the central region, and vegetation had gradually grown, because some agricultural lands had transited to vegetation. Figure 6 (m)–(o) show that the rainfall trends were similar in 2002 and 2007 that the ACR in Zigui County was more abundant than in Badong County, and the area with the most rainfall was in the southern part of Zigui County. However, in 2017, the maximum ACR transferred to Badong County.

Segmentation of slope units

LSE is conducted based on the evaluation units; thus, rational units have a direct influence on the accuracy of LSE. Grid unit is generally used in the present researches (Guzzetti et al. 1999; Hassani and Ghazanfari 2008; Cama et al. 2016; Zêzere et al. 2017; Ba et al. 2018); however, as indicated in some previous studies (Rowbotham and Dudycha 1998; Drăguț and Blaschke 2006; Blaschke and Strobl 2015), there are two main disadvantages for grid unit: (1) Grid unit does not make use of the spatial context and the terrain characteristic. However, landslide susceptibility is the spatial probability of landslide occurrence (Guzzetti et al. 2006; Blaschke and Strobl 2015), and is to a large extent constrained by the terrain conditions; therefore, spatial context and topography feature are very important for the accuracy of LSE; (2) LSE results based on grid unit often appear broken and discontinuous, and the susceptibility values of these small broken regions are usually not consistent with the actual situation.

In order to take the spatial context and terrain features into account, slope unit is employed in this work. Slope unit has two advantages: (1) Among various controlling or triggering factors, the developments of rivers and valleys have obvious inducing or controlling effects on the formation of landslides and collapses (Yang 2017). Since slope units are based on drainage and divide lines, they can comprehensively reflect the effects of drainage and terrain and thus tend to generate a more rational LSE result; (2) Compared with grid unit, slope unit can achieve a much more continuous LSE result and significantly reduce the number of evaluation units (a few million grid units were merged into 22,000 slope units in this work); thus, the evaluation efficiency is obviously increased.

By far, the most common segmentation method of slope unit is to delineate local catchments by use of flow modeling (Giles and Franklin 1998; Romstad and Etzelmüller 2009). This method generally adopts DEM and reversed DEM data to obtain the divide and drainage lines. After combining the watershed polygons respectively obtained from the DEM and reversed DEM data, each original polygon is divided into the left and right parts, and these two parts represent two slope units (Giles and Franklin 1998; Xie et al. 2003; Dymond et al. 1995; Yang 2017). Nevertheless, the disadvantages of this method are also obvious. Most of the parameters used in this method are determined by experience. Even if the values of these parameters are rationally set, a lot of cumbersome manual operations are still necessary in the later stage to get a reasonable division result.

Therefore, a method named mean-curvature watersheds was put up (Romstad and Etzelmüller 2009; Romstad and Etzelmüller 2012). Its specific segmentation process is shown in Fig. 7. In the mean-curvature map, the closed depression is commonly

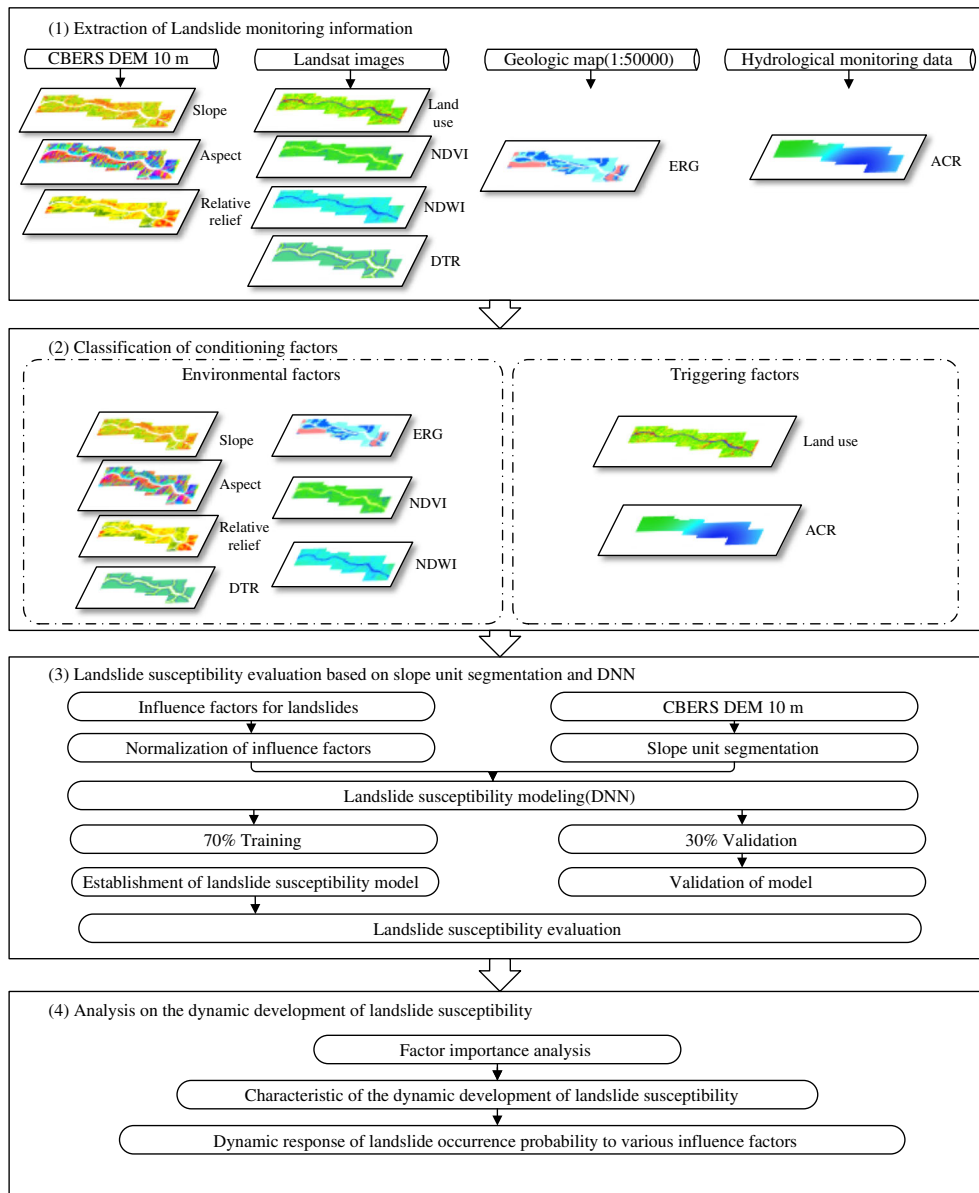


Fig. 4 Overall flowchart of dynamic evaluation of landslide susceptibility

interpreted as a topographic concave unit, and the convex unit can be generated in the same way by DEM inversion (Subtracting the DEM value from the DEM maximum of the full map), so the slope unit can be produced by their combination (Romstad and Etzelmüller 2009; Romstad and Etzelmüller 2012). However, this method is found more suitable for small-area regions; when used in a large-area region, it is apt to over-segmentation and generating broken and meaningless units. To improve it, an elimination method is used in this research. Different from the predecessor method (Romstad and Etzelmüller 2009; Romstad and Etzelmüller 2012), the smoothing procedure of the original DEM data is abandoned. The final result of the reasonable slope units is generated by eliminating the slope units smaller than the set threshold and by combining the small units with their surrounding larger slope units. Figure 8 shows the effect of the elimination method that many broken and meaningless units are deleted and more rational

slope units are acquired. Moreover, the mean filtering operation is not conducted in this research, because we found the smooth filtering would erase some important topographical features. Thus, in this work, the segmented slope units without smoothing the DEM data are hopeful to be more consistent with the actual terrain.

Deep neural networks

With the advent of the big data era, deep learning technology has become a research hotspot in the field of artificial intelligence. The learning ability of deep neural networks is superior to the traditional machine learning techniques and has been proved in many fields (Cui et al. 2014; He et al. 2015; Xing et al. 2016; He et al. 2018; Jo et al. 2018).

A deep neural network (DNN) is a multi-layer perceptron (MLP) with more than one layer of hidden units between its inputs

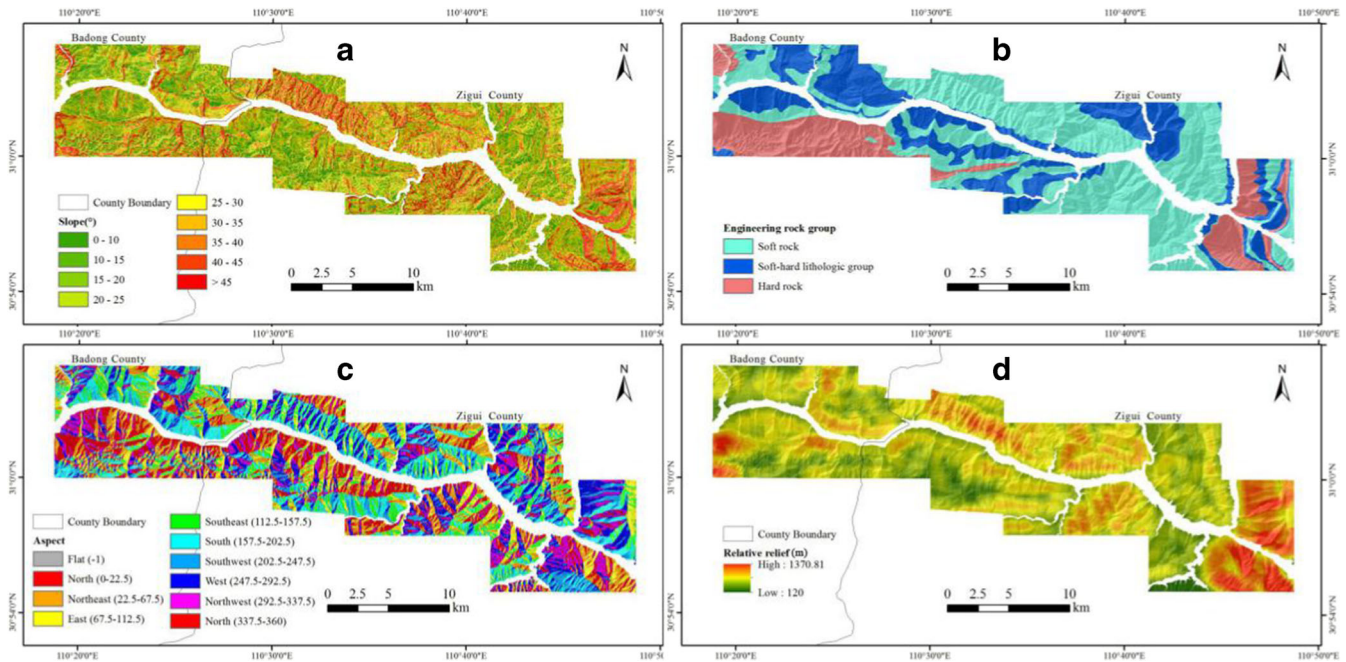


Fig. 5 Geological and environmental static factors for landslides. The background map is the shaded relief map produced from the DEM data. (a) Slope; (b) engineering rock group (ERG); (c) aspect; (d) relative relief

and outputs, and the network is optionally initialized by using the Dynamic Bayesian Network (DBN) pre-training algorithm (Malsburg 1986; Hinton et al. 2012; Seide et al. 2012). DNNs are also called full connected networks, and each node of the fully connected layer is connected to all the nodes of the previous layer to combine the features extracted from the front layer (Xu et al. 2015) (Fig. 9).

In the fully connected neural network suggested in this work, the activation function of “ReLU” is employed to introduce the nonlinear features into the network, so that the network can approach nonlinear functions (Hinton et al. 2012). The “ReLU” function is used to activate the function after linear combination to complete a nonlinear transformation (Eq. 1 and Eq. 2) (Hongyo et al. 2019; Shi et al. 2019).

$$z = \sum_{i=1}^n w_i x_i + b \quad (1)$$

where z represents the result of linear combination, w_i represents the weight of each neuron, x_i represents each neuron, and b represents a random value (*bias*).

$$\text{ReLU}(x) = \begin{cases} x & \text{if } x > 0 \\ 0 & \text{if } x < 0 \end{cases} \quad (2)$$

where x represents the input value of the function, and in most cases, x is the result of a linear combination (i.e., z in Eq. 1). When $x < 0$, “ReLU” function determines it has no value, so the output value is equal to 0. When $x > 0$, “ReLU” function will output its value.

Three $9 \times 10 \times 15 \times 6 \times 2$ (one input layer (9 nodes), three hidden layers (10 × 15 × 6 nodes) and one output layer (2 nodes)) deep neural networks are established for landslide susceptibility analysis. Each DNN corresponds to the LSE in one year (2002, 2007, or

2017). Thus, the three DNNs have the same structure of $9 \times 10 \times 15 \times 6 \times 2$, but possess different model parameters (e.g., input database, model weights, and output database). With regard to each DNN, the 9 input nodes represent the 9 landslide influence factors (land use, aspect, ERG, slope, DTR, relative relief, NDWI, NDVI, and ACR) of a certain year (2002, 2007, or 2017). The output of DNN is the landslide susceptibility in the corresponding year. The numbers of nodes in the three hidden layers are 10, 15, and 6, respectively. After each layer of neurons is calculated, the activation function of “ReLU” is used to complete a nonlinear transformation from the values of the nine influence factors to the output variables. Then, the “Sigmoid” function (Shi et al. 2019; Oysal 2005) is used to map the output variables to the values of 0 (no landslide) and 1 (landslide). However, LSE reveals the probability of slope failure, so the prediction result of the DNN should be the values between 0 and 1. Thus, an error function (Eq. 3 and Eq. 4) (He et al. 2019) is constructed in this study to guarantee the output values varying from 0 to 1, rather than 0 or 1. The principle of the error function is that the power of $(y - \bar{y})$ is 4, so the predicted value between 0 and 1 will have a smaller loss. For example, the value of a loss function that predicts the value 0 as 1 is much larger than the value of a loss function that predicts the value 0 as 0.2 (i.e., $(0.2-0)^4 \ll (1-0)^4$). Deep learning is mainly learned by lowering the loss function value (Xing et al. 2016), so the value by using 0.2 instead of 1 will be chosen as the prediction result. Thus, in the effect of the error function, the final result can be transformed into the probability value of landslide occurrence. Furthermore, many DNNs use the power of 2 (e.g., Hinton et al. 2012; Meier and Masci 2012; Toshev and Szegedy 2013; Xu et al. 2015; Havaei et al. 2017), whereas this work employs 4 as the power value because the larger power value can further reduce the value of the loss function. The output layer contains two values, one is

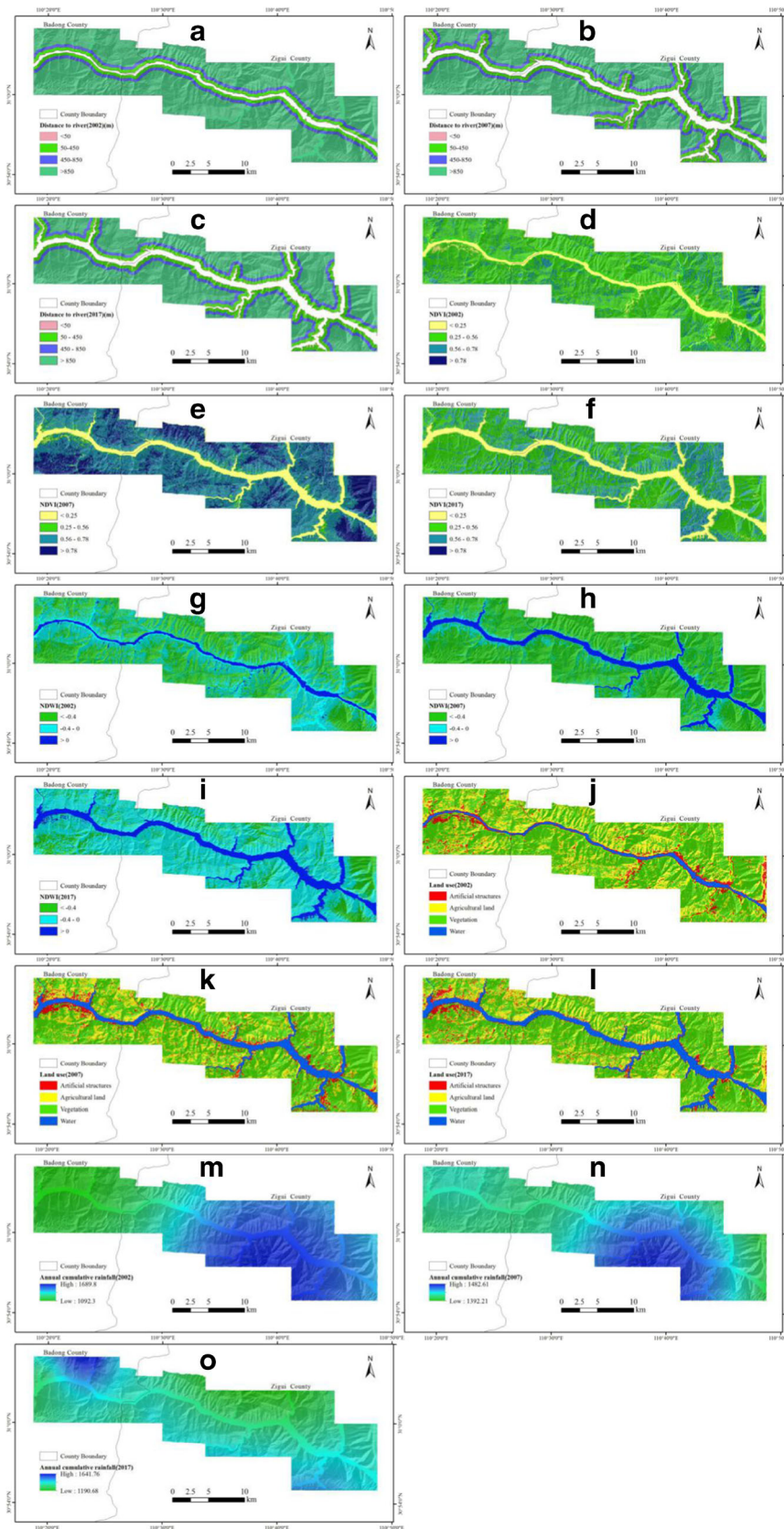


Fig. 6 Dynamically changing influence factors in the study area. These factors include geological and environmental dynamic factors and triggering factors. The factor maps are superimposed on the shaded relief map produced from the DEM data. (a) Distance to river (DTR) in 2002; (b) DTR in 2007; (c) DTR in 2017; (d) normalized difference vegetation index (NDVI) in 2002; (e) NDVI in 2007; (f) NDVI in 2017; (g) normalized difference water index (NDWI) in 2002; (h) NDWI in 2007; (i) NDWI in 2017; (j) land use in 2002; (k) Land use in 2007; (l) land use in 2017; (m) annual cumulative rainfall (ACR) in 2002; (n) ACR in 2007; (o) ACR in 2017

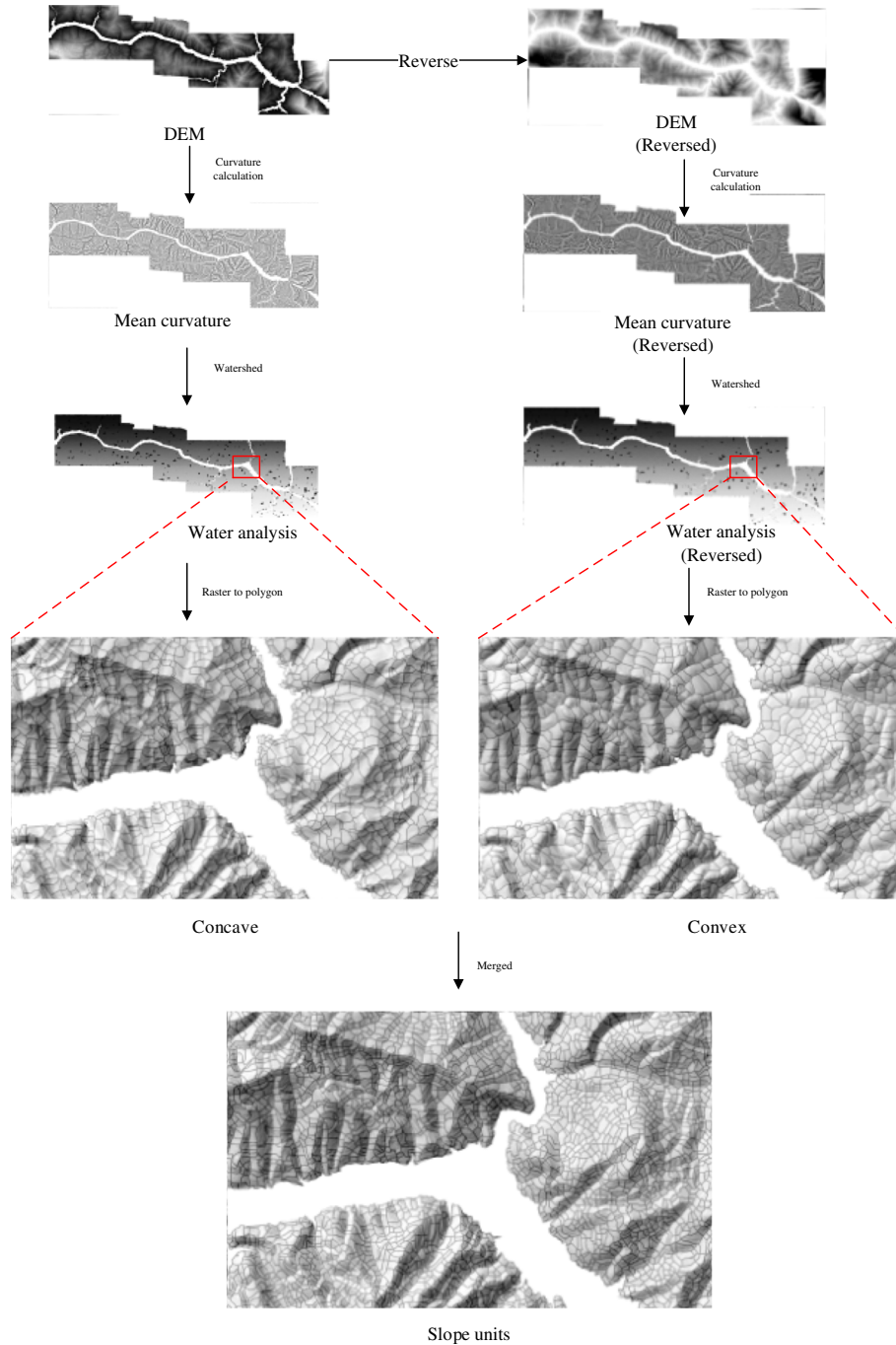


Fig. 7 Procedures of slope unit segmentation (Romstad and Etzelmüller 2009; Romstad and Etzelmüller 2012). The segmentation maps are all superimposed on the shaded relief map produced from the DEM data

the probability that a landslide will occur, and the other is the probability that no landslide will occur. The two values add up to 1.

$$e = (y - \bar{y})^4 \tag{3}$$

where y represents the calculated value, \bar{y} represents the actual value, and e represents the error of a single calculated value.

$$\begin{aligned}
 E &= \frac{1}{n} (e^{(1)} + e^{(2)} + e^{(3)} + \dots + e^{(n)}) \\
 &= \frac{1}{n} \sum_{i=1}^n e^{(i)} \\
 &= \frac{1}{n} \sum_{i=1}^n (y^{(i)} - \bar{y})^4
 \end{aligned} \tag{4}$$

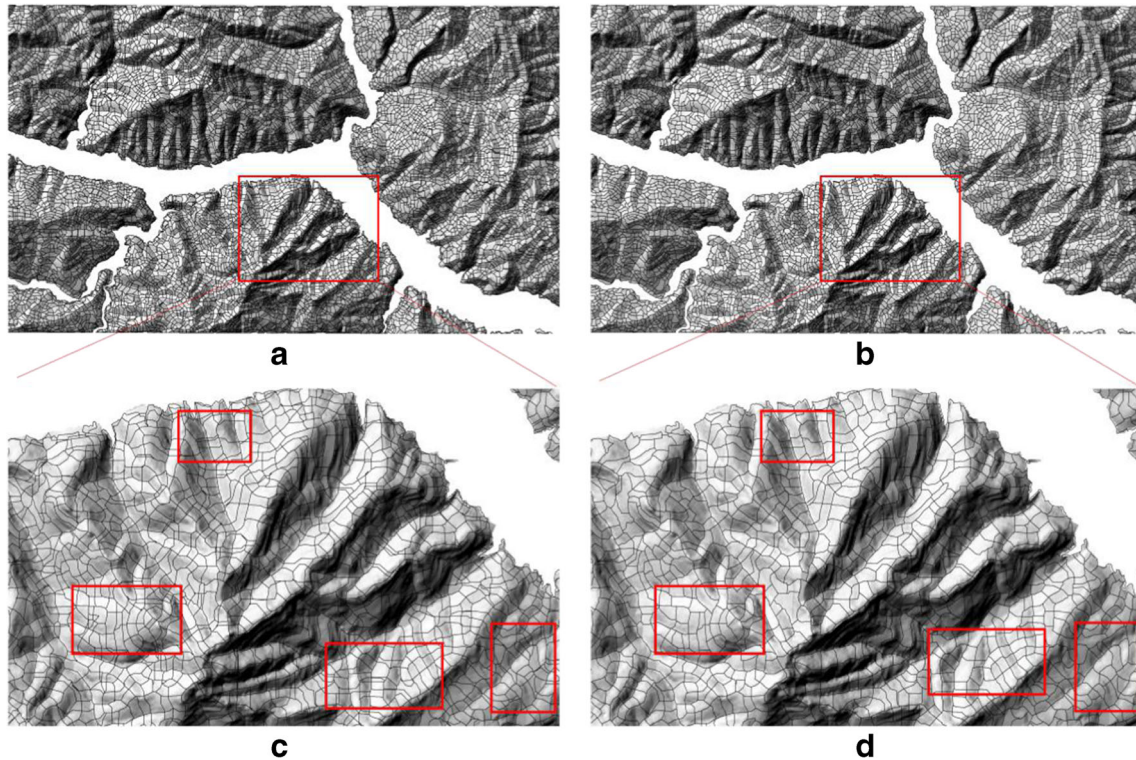


Fig. 8 Segmentation of slope units before and after elimination of small units. The segmentation maps are all superimposed on the shaded relief map produced from the DEM data. (a) Segmentation of slope units before elimination of the small units. (b) Segmentation of slope units after eliminating the small units. (c) Partial enlarged details of the segmentation map (a). (d) Partial enlargement of the segmentation map (b)

where e^i represents the error of each calculated value (Eq. 3), n represents the number of the calculated values, and E represents the loss function value while deep learning is mainly learned by lowering the E value.

Therefore, for each year, the values of the nine influence factors in each slope unit are input into the constructed DNN, and then the landslide susceptibility in each slope unit is output to obtain the landslide susceptibility in the whole region. Thus,

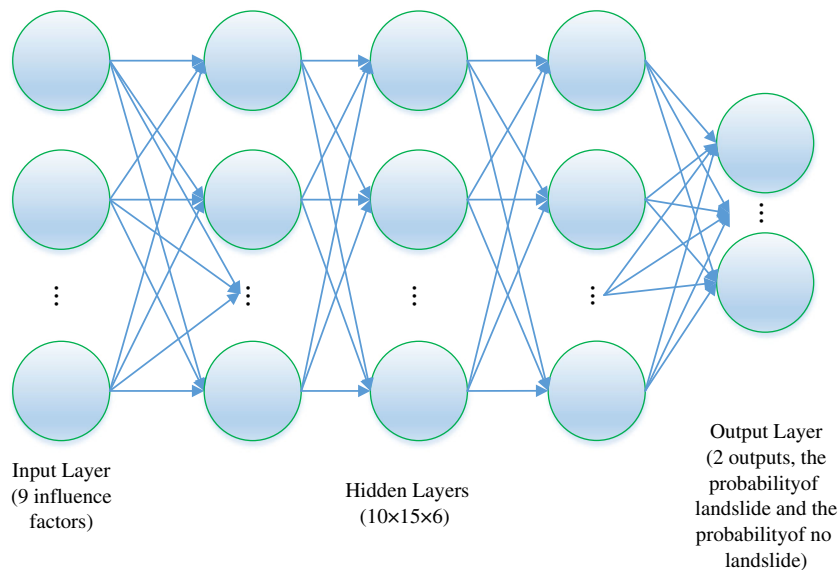


Fig. 9 Structure of deep neural networks in this study

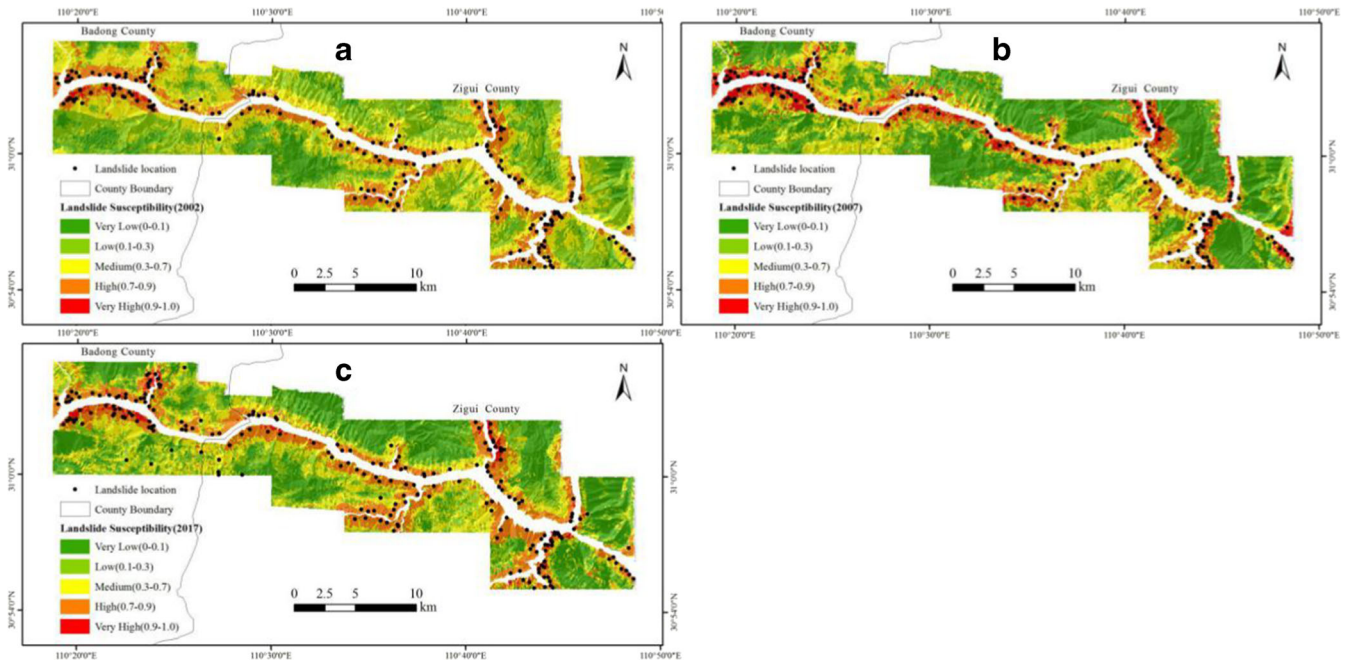


Fig. 10 Landslide susceptibility maps. The back map is the shaded relief map produced from the DEM data. (a) Landslide susceptibility in 2002; (b) landslide susceptibility in 2007; (c) landslide susceptibility in 2017

the landslide susceptibility maps of the study area in 2002, 2007, and 2017 are generated based on slope unit and DNN.

Results

Landslide susceptibility evaluation

The maps of LSE in 2002, 2007, and 2017 are shown in Fig. 10. The landslides are mainly distributed in the high-susceptibility and very high-susceptibility areas, which proves the rationality of the landslide susceptibility results. The number of the landslide units falling in each susceptibility level is counted and shown in Table 3.

Table 3 shows that in the 3 years, the numbers of landslide slope units falling in the “very low” and “low” regions are 13, 11, and 16, accounting for only 0.59%, 0.50%, and 0.71% of the total landslide units, respectively. Moreover, most of the landslide slope units are located in the “high” and “very high” regions, accounting for 73.37%, 83.45%, and 82.57% of all landslide units, respectively.

As shown in Table 4, from 2002 to 2007 then to 2017, the proportion of high and very high susceptibilities showed an increasing trend. However, the “very high” area in 2007 was significantly higher than in 2002 and 2017, and the fluctuation of reservoir water level may have played an important role in the dynamic change of landslide susceptibility. The specific cause of

the landslide susceptibility change and its relation to reservoir water level are analyzed in the “Discussions” section.

Precision evaluations

The known samples are segmented to 70% training samples and 30% validation samples. Both the training and validation samples are sourced from landslide and non-landslide samples with the proportion 1:1. Both landslide and non-landslide samples are randomly selected in the study area, and the buffer technique is employed to keep the non-landslide samples at least 1 km away from the landslide areas. Zhu et al. (2019) suggested a new and attractive sampling strategy based on the dissimilarity in the environmental conditions between the non-landslide and landslide samples. This new sampling method improves the reliability of the generated non-landslide samples and may possess a better performance for LSE than the buffer-controlled sampling. Thus, the new strategy may be incorporated in our future work to further improve the accuracy of LSE.

The validation samples are not used to construct the LSE DNN model, so they are employed to verify the accuracies of the LSE results. As Fig. 11 shows, the ROC curves for the 3 years are generally similar, and the AUC values are 0.983, 0.984, and 0.977, respectively. In addition, statistical analysis is also conducted to

Table 3 The number of the landslide slope units falling in each susceptibility level. PLHVH means the proportions of the landslide units in the high and very high susceptibility areas to all landslide units

	Very low	Low	Medium	High	Very high	Total	PLHVH (%)
2002	0	13	576	1496	127	2212	73.37
2007	1	10	355	1050	796	2212	83.45
2017	3	13	374	1611	237	2238	82.57

Table 4 Areas and proportions of high and very high susceptibilities and the reservoir water level in each year

	Very high susceptibility (km ²)	High and very high susceptibilities (km ²)	Total area of five susceptibility levels (km ²)	Reservoir water level (m)	Proportion of high and very high susceptibilities (%)
2002	3.43	75.32	400.77	66	18.79
2007	31.51	89.07	400.77	156	22.22
2017	7.25	95.02	400.77	175	23.71

evaluate the precisions of the LSE results in this work, and the statistical indexes include Accuracy ACC, *F* measure, root mean squared error (RMSE), Kappa, area under curve (AUC), and true positive rate (TPR) (Table 5).

Therefore, the generated landslide susceptibility maps may have a high credibility according to the relatively high values of various accuracy indexes, the majority of landslides distributed in the high and very high susceptibility regions, as well as the areas of the high and very high susceptibility regions.

Effect of the DNN parameters

Regarding the establishment of the DNN-based LSE model, there are primarily two parameters: one is the ratio of the training and validation samples, and the other is the batch size. Batch size is used in batch normalization to avoid overfitting by normalizing inputs of each layer (Kim et al. 2017).

To explore the effects of the two parameters on the LSE results, two charts (Figs. 12 and 13) are used to highlight the best parameter values. As Fig.12 shows, although the ratio of 70%:30% possesses a lower training accuracy of 2007 than the ratio 50%:50%, it has the highest training and validation precisions for all the other years. Based on the integration performance and the validation accuracies, the ratio 70%:30% is employed in this work. As Fig. 13 shows, e.g., the accuracies of 2017, the training accuracy achieves the highest two values (0.945 and 0.946) when the batch size equals to 600 and 1000, respectively. However, the validation precision attains the highest value when the batch size is 600, and the validation accuracy when the batch size is 600 is significantly higher than the one when the batch size is 1000. The precisions

of 2002 and 2007 have a similar trend that the validation precisions reach the highest values when the batch size equals to 600. Therefore, the batch size of 600 is selected in this work.

Model comparison

As suggested by some researches (Cao et al. 2019b; Chen et al. 2014; Hu et al. 2019; Stumpf and Kerle 2011; Wang et al. 2019b), random forest (RF), support vector machine (SVM), and logistic regression (LR) are excellent machine learning algorithms. Thus, in this work the DNN LSE model is compared with the above three models of RF (Breiman 2001), SVM (Chapelle et al. 1999), and LR (Young et al. 1993). Figure 14 shows the comparison of the LSE accuracies by using the training samples, and Fig.15 presents the comparison of the LSE precisions by using the validation samples. Thus, Figs. 14 and 15 show the training accuracies and the verification accuracies, respectively. The validation samples are not adopted to construct the LSE models, so compared with the training samples, they can better reflect the generalization ability and the prediction accuracy of a LSE model. Moreover, the LSE maps of the above three models are shown in Fig.S1 and Fig.S2 in the supplementary file.

As shown in Figs. 14 and 15, although RF possesses slightly higher training accuracies than DNN, DNN has higher verification accuracies than RF. Therefore, DNN has a better performance to overcome the overfitting problem and possesses a better generalization ability and higher evaluation accuracies of landslide susceptibility. DNN performs better than the other three models in the study area. Nevertheless, RF is also an outstanding machine learning algorithm and achieves higher evaluation precisions than SVM and LR in the study area.

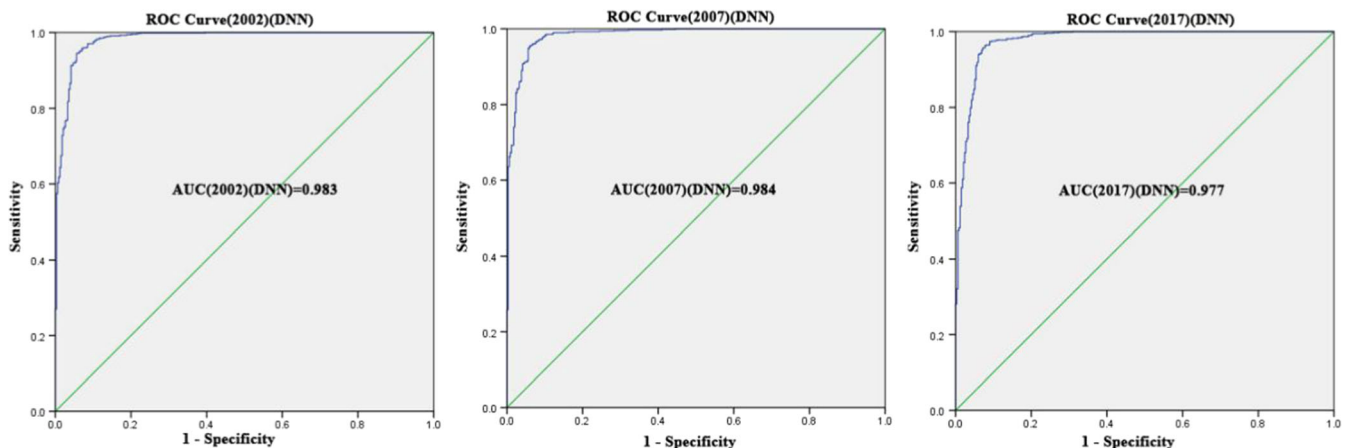


Fig. 11 Receiver operating characteristic (ROC) curves of landslide susceptibility evaluations for the 3 years of (a) 2002, (b) 2007, and (c) 2017. AUC is the abbreviation of the area under the ROC curve. The ROC plots are drawn with the SPSS statistics software (Version 20.0)

Table 5 Accuracies of the LSE results for the 3 years. TP, FP, TN, and FN mean true positive, false positive, true negative, and false negative, respectively. Accuracy ACC (%), *F* measure, Kappa are the statistical indexes for precision evaluation. RMSE, AUC, and TPR mean root mean squared error, area under curve, and true positive rate, respectively

		DNN(2002)	DNN(2007)	DNN(2017)
Binary prediction results	TP	653	651	658
	FP	17	19	18
	TN	305	308	303
	FN	34	31	30
Accuracy indexes	Accuracy ACC (%)	94.95	95.04	95.24
	<i>F</i> measure	0.962	0.963	0.965
	RMSE	0.225	0.223	0.218
	Kappa	0.885	0.888	0.891
	AUC	0.983	0.984	0.977
	TPR (%)	95.05	95.45	95.64

Discussions

Which key factors influence landslide susceptibility?

Significance and contribution of various influence factors are analyzed (Fig. 16). The main factors affecting landslide occurrence are DTR, NDWI, relative relief, and ERG (Fig. 16). Among them, DTR ranks first for all the 3 years; thus, the change of reservoir water level has a crucial impact on landslide occurrence. As mentioned above, in 2002, 2007, and 2017, the maximum water levels were 66 m, 156 m, and 175 m, respectively (Table 1). The change of the reservoir water level is unfavorable to the stability of the local slopes, especially when large rising or falling of the water level in a short period (TGWC, Three Gorges Reservoir Area Geological Disaster Prevention and Control Work Command 2010). When the water level rises, the shearing strength of the slope is reduced due to the immersion (Miao et al. 2014). When the water level drops, the pore water in the slope cannot rapidly drain, so that the water level in the slope is higher than the reservoir water level, which reduces the anti-sliding ability of the potential sliding surface (Paolo et al. 2013;

Zhou et al. 2014). Therefore, in the Three Gorges Reservoir area, the change of reservoir water level has the greatest impact on landslides.

Figure 16 (b) shows the total significance values in the 3 years. DTR still contributes most to landslide occurrence and development in the study area. With regard to the significant geoenvironmental factor of NDWI, it reflects soil moisture. Soil water content affects soil cohesion and thus changes soil shear strength (Gaudio et al. 2013; Ruetter et al. 2013). With regard to the factor of ERG, a crucial control factor for landslides, it indicates the structural property of rocks. The rock mass on the slope often undergoes plastic deformation and damage under the setting of soft rock and soft layer (Wu et al. 2013; 2014), which may result in landslides. Thus, the landslides in the study area are mainly distributed in the region with the lithology of soft rock or soft-hard interbedded rock (Fig. 5 (b)). As for the factor of relative relief, it to some degree delineates the type of landform. When the local type is cutting hills or loess and the gullies are extremely developed, it provides convenient conditions for the development of landslides (Saha et al. 2005; Chauhan et al. 2010).

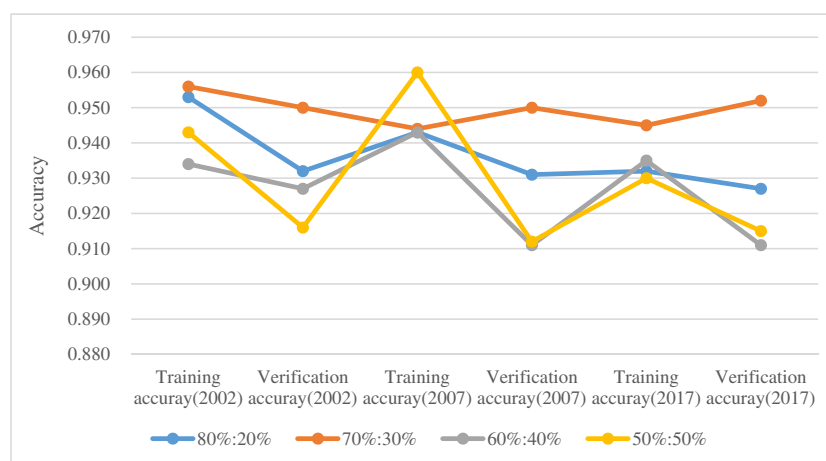


Fig. 12 Training and validation accuracies of 2002, 2007, and 2017 under three different ratios of training and validation samples

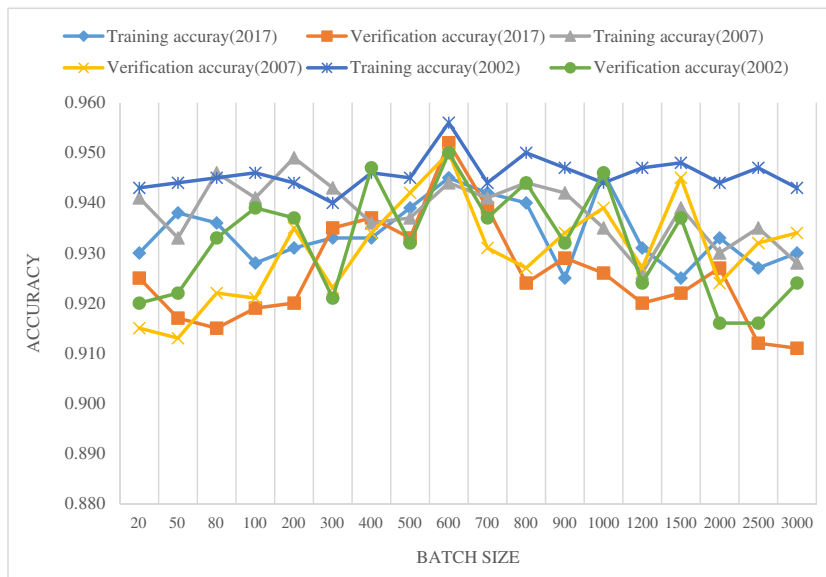


Fig. 13 Training and verification accuracies under different batch sizes

What are the development characteristics of landslide susceptibility in the study area?

As shown in Fig. 17, from 2002 to 2007, the newly added high-landslide-susceptibility (HLS) areas were mainly distributed along the Yangtze River and its tributaries. From 2007 to 2017, the distribution of new HLS areas became different, and the mountainous areas far from the Yangtze River also presented an increase in landslide occurrence probability.

The slope units with the susceptibility changing level equal to or larger than 2 and the constructed road networks are extracted to analyze the distribution features of the newly added HLS areas (Fig. 18). From 2002 to 2007, most of the new HLS areas were

distributed along the Yangtze River, some else were distributed around the roads, and few were situated on the mountains far from the roads. From 2007 to 2017, more than half of the new HLS areas were distributed nearby the road networks, some else were located in the mountainous areas far away from the roads in Zigui County, and few of them lay along the Yangtze River. The mountainous regions associated with the new HLS areas were generally characterized by the increase of the soil moisture content, and the soil water content is closely related to rainfall.

Figure 19 shows the changing trend of landslide susceptibility. The susceptibility evolutionary trends appear generally consistent from 2002 to 2007 and from 2007 to 2017. The susceptibility kept

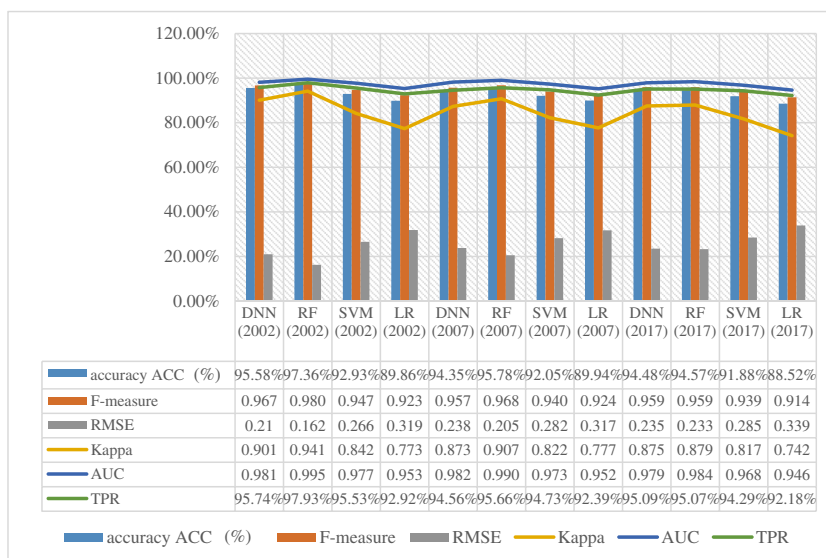


Fig. 14 Comparison of four models in training accuracies. RMSE, AUC, and TPR mean root mean squared error, area under curve and true positive rate, respectively. RF, SVM, LR mean random forest, support vector machine, and logistic regression, respectively

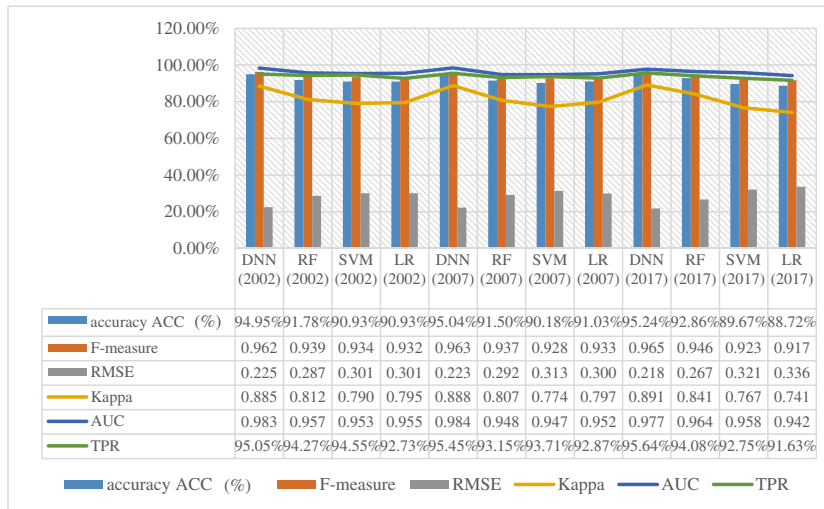


Fig. 15 Comparison of four models in verification accuracies. RMSE, AUC, and TPR mean root mean squared error, area under curve and true positive rate, respectively. RF, SVM, LR mean random forest, support vector machine, and logistic regression, respectively

unchanged in about 46.61% and 45.85% areas from 2002 to 2007 and from 2007 to 2017, respectively. The regions with minor susceptibility changes (the changing level equals to ±1) occupy approximately 48.37% and 46.78% of the study area from 2002 to 2007 and from 2007 to 2017, respectively. Only in rare regions, about 5.02% from 2002 to 2007 and 7.37% from 2007 to 2017, the susceptibility obviously decreased or increased (with the absolute values of the changing level equal to or larger than 2).

To better reflect the relation between reservoir water fluctuation and landslide susceptibility variation, Fig. 20 shows the changing trend of landslide susceptibility within the reservoir water fluctuation area (DTR < 100 m). From 2002 to 2007, the susceptibility increased in 39.04% of the fluctuation area (the susceptibility rising level equals to 1 or 2); thus, the change of reservoir water level had a significant impact on the landslide occurrence probability along the reservoir bank. The rising of the reservoir water level from 66 to 156 m led to the increase of landslide occurrence probability along the reservoir bank. From 2007 to 2017, the area with decreasing landslide occurrence

probability was larger than the one with increasing landslide occurrence probability, and the two types of areas occupied 27.03% and 17.94% of the reservoir water fluctuation region, respectively. Thus, under the attention and disaster control of the government, especially under the control of the landslides on both sides of the reservoir bank, the rising of water level from 156 m to 175 m and the later periodic fluctuation had less influence on the rise of the landslide occurrence probability along the reservoir bank.

As shown in Fig. 21, from 2002 to 2007, the increase in NDWI values mainly occurred in the area along the Yangtze River, as a result of the rise of water level and the emergence of tributaries (Fig. 6 (a)–(c)). The red in Figure 21 (a) indicates the area with obviously increasing NDWI values (the changing level equals to 2), and the area also corresponds to the region where the ground was flooded and the new tributaries appeared after the rise of reservoir water level. According to the change of landslide susceptibility, from 2002 to 2007, the increase of landslide occurrence probability along the Yangtze River resulted from the increase of NDWI. Therefore, from 2002 to 2007,

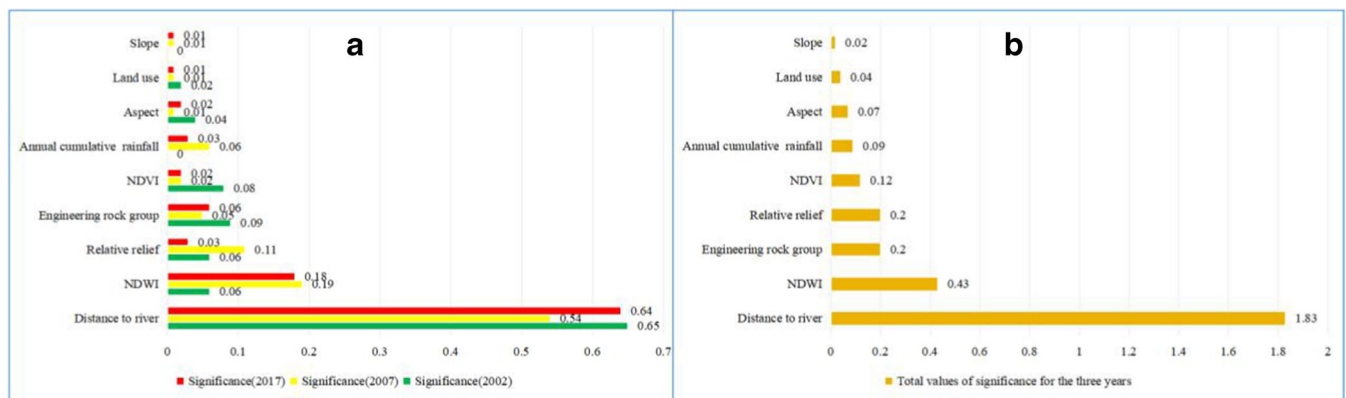


Fig. 16 Significances and contributions of various influence factors. (a) Significance values of various influence factors in each year. (b) Total significance values of various influence factors in the 3 years. The significance analysis is conducted by the sensitive analysis method of SPSS Modeler software (Version 18.0)

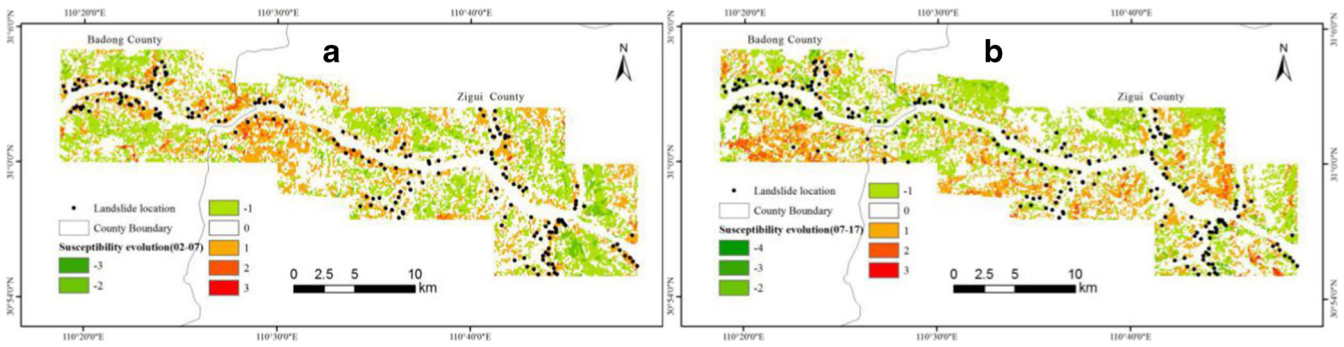


Fig. 17 Dynamic change of landslide susceptibility (a) from 2002 to 2007 and (b) from 2007 to 2017. The value indicates the varying degree of landslide susceptibility. For example, 2 denotes the susceptibility level changing from low to high levels or from very low to medium levels or from medium to very high levels, and -3 represents the susceptibility level changing from very high to low levels or from high to very low levels

landslide occurrence probability along the Yangtze River increased due to the rise of the reservoir water level. The red and orange area in Fig. 21 (b) occupies almost the entire study area, which illuminates that the soil water content in almost all the study area increased. According to the meteorology monitoring data from Hubei Provincial Hydrology and Water Resources Bureau (<http://113.57.190.228:8001/web/Report/CantonRainSta>), rainfall occurred in the study area on February 20 to 25, 2017. Since the remote sensing image was shot on March 2, 2017, the increase in NDWI values in the region may have been caused by rainfall. Thus, the increase of landslide occurrence probability in the mountainous areas far from the Yangtze River resulted from rainfall.

In conclusion, from 2002 to 2007, the new HLS areas mainly appeared along the Yangtze River and also distributed around the roads. From 2007 to 2017, more than half of the new HLS areas were situated around the roads, and the increase of landslide susceptibility also occurred in the mountainous areas far from the Yangtze River. Therefore, from 2002 to 2007, the change in landslide occurrence probability was mainly caused by the combined effect of reservoir water level fluctuation and road construction. From 2007 to 2017, the variation in landslide occurrence probability was mainly caused by the combined impact of rainfall and road construction.

What are the dynamic responses of landslide occurrence probability to various changing factors?

The dynamic responses of landslide occurrence probability to various changing factors actually refer to the relation between the development of landslide susceptibility and the variation of various changing factors. How does landslide susceptibility develop with the changing of various influence factors?

There are five changing factors of DTR, NDWI, NDVI, ACR, and land use. As revealed in “What are the development characteristics of landslide susceptibility in the study area?” the main factors influencing development of landslide occurrence probability are DTR, road construction, and NDWI.

As for DTR, it reflects the effect of reservoir water fluctuation. When the water level rises, the strength of the rock mass below the water level will decrease rapidly under the softening effect of water (Paolo et al. 2013). Also, the submerged part will be affected by the floating force, and the active weight of the soil will decrease (Zhou et al. 2014). Thus, the anti-sliding force of the slope body will reduce and the probability of landslide occurrence will correspondingly increase (Paolo et al. 2013; Miao et al. 2014). When the water level drops sharply, the reservoir water level decreases faster than the groundwater level in the slope, and then the groundwater level and the reservoir water level form a positive drop (Paolo et al. 2013; Miao

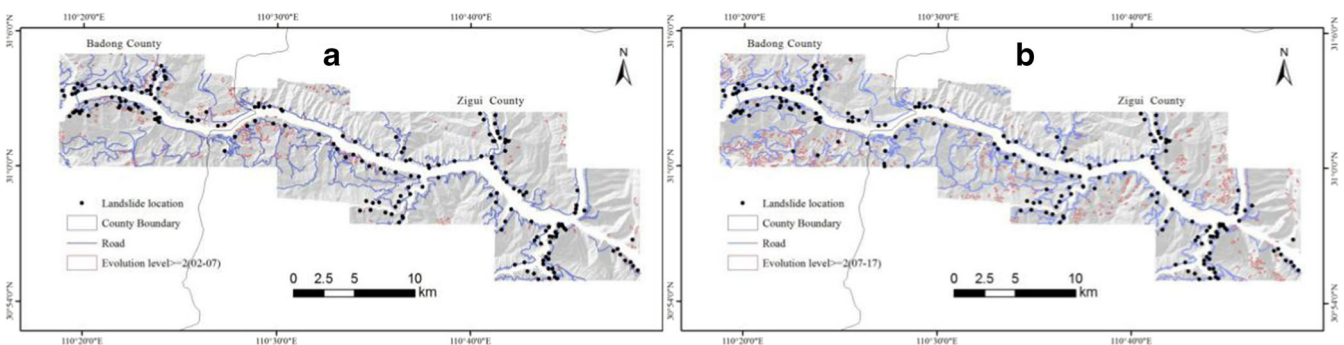


Fig. 18 Distribution of slope units with the susceptibility changing level equal to or larger than 2 and the constructed road networks in the study area. The road networks are extracted from the Google images (images.google.com.hk) and the Landsat images (<http://www.gscloud.cn/>). The Google images were shot on August 27, 2007, April 14, 2015, and October 9, 2017, respectively. The Landsat images were acquired on March 9, 2002, August 17, 2007, and March 2, 2017, respectively. The back map is the shaded relief map produced from the DEM data

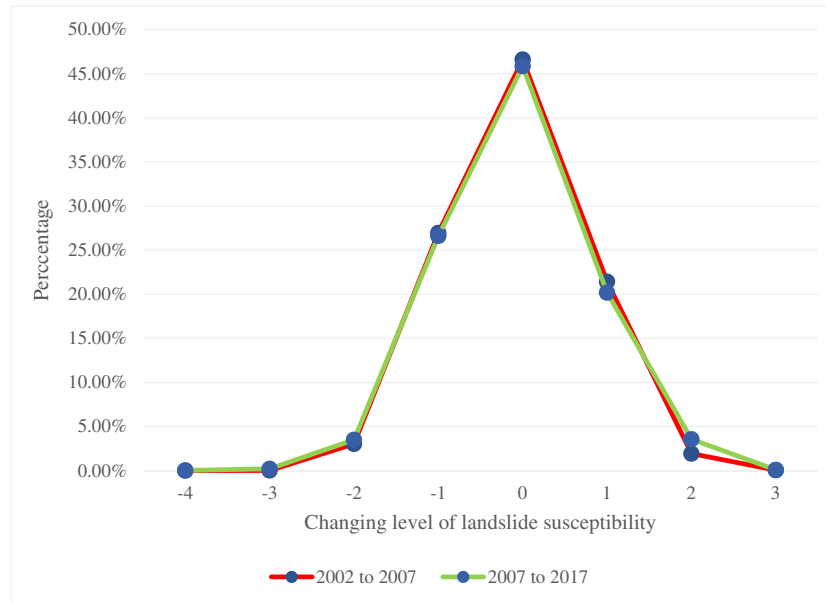


Fig. 19 Changing level of landslide susceptibility

et al. 2014; Zhou et al. 2014). The hydrodynamic pressure increases and points to the outside of the slope, causing the augment of landslide susceptibility (Miao et al. 2014). As mentioned above, in order to ensure the smooth running of the Three Gorges Dam, the reservoir water level has periodically fluctuated after the completion of the Three Gorges Reservoir. Therefore, as the reservoir water level increased during the period from 2002 to 2007, the influence range of reservoir water fluctuation also increased, thus enhancing the landslide susceptibility along the reservoir bank. From 2007 to 2017, under the control and cure measures of the government to the landslides along the reservoir bank, the rise and fluctuation of the reservoir water level did not result in the distinct increase of landslide susceptibility along the bank.

As for road construction especially from 2007 to 2017, the soil at the slope foot was excavated downwards; thus, it may have increased the slope height and weakened the counterpressure of the slope foot (Anno 1993; Kamp et al. 2008). Therefore, the stress in the slope was redistributed and adversely affected the slope stability (Anno 1993; Kamp et al. 2008). Moreover, the stress redistribution of the slope soil caused the protogenous closed cracks to open

in silty clay. The serious cut of the soil masses provided convenience for water penetration via the cracks and for the formation of underwater seepage channels (Kamp et al. 2008; Owen et al. 2008). As shown in Fig. 18, the increases of landslide susceptibility, especially from 2007 to 2017, were evidently partly caused by the road construction. There is an obvious special coherence between the areas with increasing susceptibility and the ones with the constructed road networks. The regions with significantly increasing susceptibility caused by road construction are highlighted in Fig. 22.

With regard to NDWI, the enhancement of landslide occurrence probability in 2017 was partly resulted from the augment of the soil water content. Soil water content affects the distributions of water infiltration and groundwater runoff during precipitation and further influences landslide occurrence probability (Gaudio et al. 2013; Ruetter et al. 2013). The rise of soil water content reduces the soil moisture absorption; in addition, under the long-term wet state, the soil particles expand and swell, which reduces the gap between particles (Montrasio et al. 2015; Thomas et al. 2018). When the soil moisture absorption exceeds its water-holding capacity,

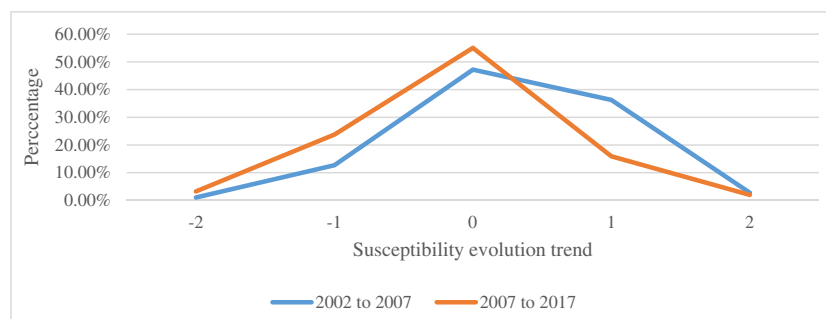


Fig. 20 Changing trend of landslide susceptibility in the reservoir water fluctuation area

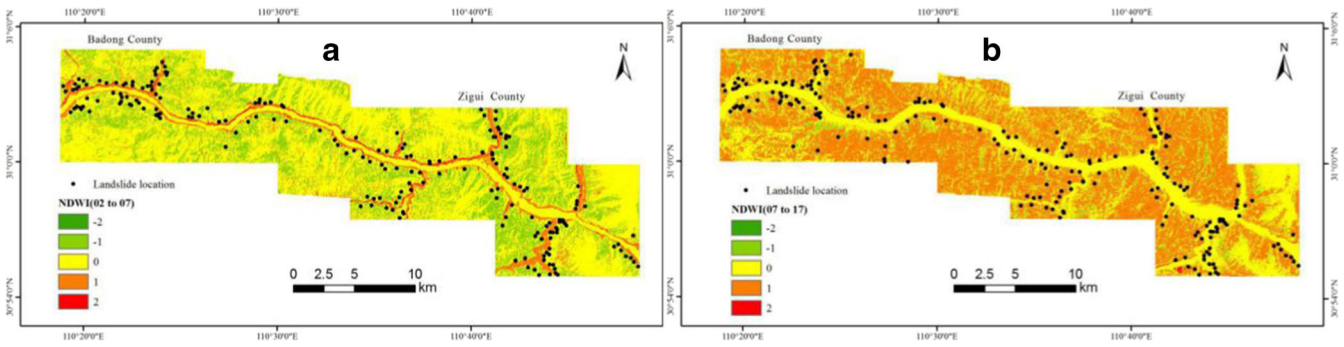


Fig. 21 Variations of normalized difference water index (NDWI) (a) from 2002 to 2007 and (b) from 2007 to 2017. The NDWI values are divided into three grades of 1, 2, and 3 representing the value ranges of < -0.4 , $-0.4\sim 0$, and > 0 , respectively. The values in the figures represent the varying levels of NDWI. For example, 2 represents the NDWI grade changing from 1 to 3, and -1 represents the NDWI grade varying from 3 to 2 or from 2 to 1

the excess water continues infiltrating and thus forms underground runoff at the interface between the bottom soil and the rock surface (Ruelle et al. 2013; Montrasio et al. 2015; Thomas et al. 2018). In this case, the anti-sliding ability of the slope body will sharply drop, and the landslide occurrence probability will increase (Montrasio et al. 2015; Thomas et al. 2018). As mentioned in “What are the development characteristics of landslide susceptibility in the study area?” rainfall occurred in the study area from February 20 to 25, 2017. According to the meteorological monitoring by Zhouping Station, even moderate rain (according to the standard of China Meteorological Administration) happened on February 21 with the daily cumulative rainfall of 18.5 mm. As a result, the soil moisture in almost all the study area increased (Fig. 21 (b)); thus, in 2017 the mountainous areas far from the Yangtze River presented an increase in landslide susceptibility. The areas with obviously rising susceptibility caused by the increase of the soil water content are illuminated in Fig. 22.

Conclusions

This work focuses on the dynamic change of landslide susceptibility and the dynamic response of landslide occurrence probability to various changing influence factors. Multi-source and three-temporal landslide monitoring data are employed to conduct LSE based on slope unit segmentation and DNNs. Four conclusions are drawn in this work.

1. The main factors affecting landslide occurrence are DTR, NDWI, relative relief, and ERG. Among them, DTR ranks first in all the three years; thus, the change of reservoir water level has the most crucial impact on landslide occurrence. NDWI manifests soil moisture, and soil water content affects soil cohesion and thus affects soil shear strength (Gaudio et al. 2013; Ruelle et al. 2013). The relative relief to some extent depicts the type of landform. When the local type is cutting hills or loess and the gullies are extremely developed, it

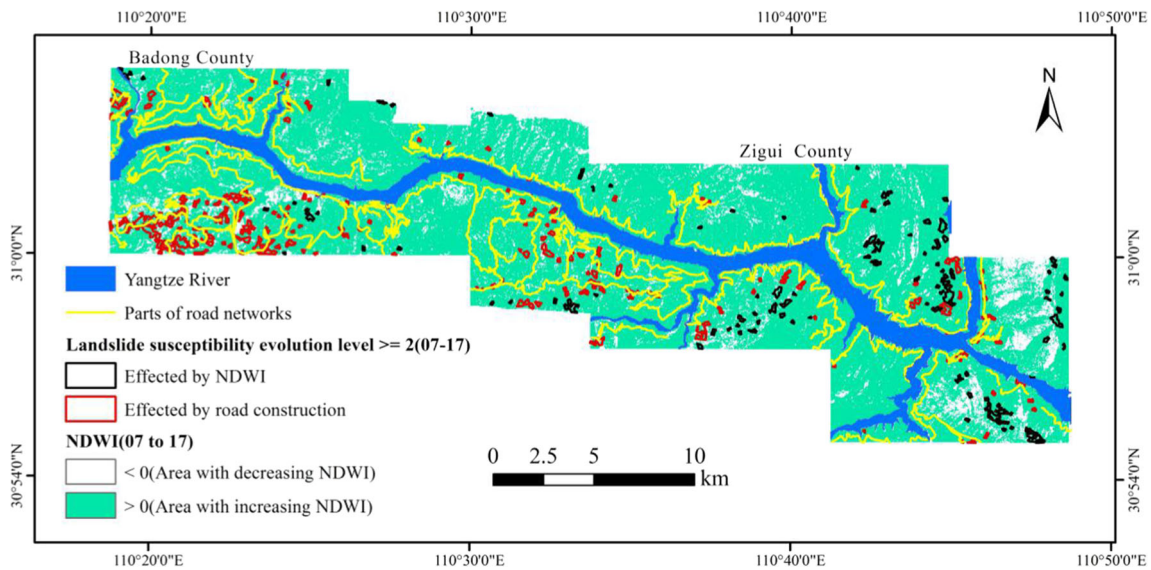


Fig. 22 Relations among the increase of landslide susceptibility, soil moisture and road networks. The regions with distinctly increasing susceptibility caused by road construction and soil moisture are highlighted by the colors of red and black, respectively. The white regions, excluding the Yangtze River, are characterized by decreasing NDWI values

provides convenient conditions for the development of landslides (Saha et al. 2005; Chauhan et al. 2010). ERG portrays the structural property of rocks. The rock mass on the slope often undergoes plastic deformation and damage under the setting of soft rock and soft layer, which may result in slope instability (Wu et al. 2013; 2014).

2. From 2002 to 2007, the new high-susceptibility areas mainly appeared along the Yangtze River and also distributed around the roads in the study area. From 2007 to 2017, more than half of the new high-susceptibility areas were situated around the roads, and the increase of susceptibility also occurred in the mountainous areas far from the Yangtze River. Therefore, from 2002 to 2007, the change in susceptibility was mainly caused by the combined effect of reservoir water level fluctuation and road construction. From 2007 to 2017, the variation in susceptibility was mainly caused by the combined impact of rainfall and road construction.
3. There are five changing factors of DTR, NDWI, NDVI, ACR, and land use. In the study area, the main factors influencing development of landslide occurrence probability are DTR, road construction, and NDWI. As for DTR, it reflects the effect of reservoir water fluctuation. As the reservoir water level increased from 2002 to 2007, the influence range of reservoir water fluctuation also correspondingly increased, which caused the rise of landslide susceptibility along the reservoir bank. As for road construction, especially from 2007 to 2017, the development of many road networks changed the stress in the slope, destroyed the original balance condition of the slope, and generated a large number of cracks, thus further increasing the probability of landslide occurrence. NDWI reflects the soil water content, and the rising of NDWI in 2017 resulted from the antecedent precipitation. Thus, the increase of landslide susceptibility in 2017 was partly caused by rainfall.
4. A combination of slope unit segmentation and DNNs can achieve a good performance in LSE. The methods suggested in this work can be generalized to other hardest hits of landslides.

Acknowledgments

1:50,000 geological map, 1:10,000 relief map, rainfall data, and most landslide investigation information are provided by the Three Gorges Reservoir Area Geological Disaster Prevention and Control Work Command (TGWC). The water level data are from the TGWC. The vector data of the administrative boundaries are downloaded from https://download.csdn.net/download/yzj_xiaoyue/10612119. The Sentinel-2A images are from <https://scihub.copernicus.eu/>. Landsat images used in this work are obtained from <http://www.gscloud.cn/>. The employed Google images are sourced from images.google.com.hk. The DEM data are from China and Brazil Earth Resource Satellite. We also appreciate Hubei Provincial Hydrology and Water Resources Bureau for providing rainfall data (<http://113.57.190.228:8001/web/Report/CantonRainSta>). This work is funded by National Natural Science Foundation of China (No. 41372341). We are much grateful for the valuable comments of the editor and the three anonymous reviewers. These comments have improved the manuscript a lot.

References

- Anno (1993) Landslide processes and landslide susceptibility analysis from an upland watershed: a case study from St. Andrew, Jamaica, West Indies. *Eng Geol* 34(1):53–79
- Ba Q, Chen Y, Deng S, Yang J, Li H (2018) A comparison of slope units and grid cells as mapping units for landslide susceptibility assessment. *Earth Sci Inf* 11(3):373–388
- Bacha AS, Shafique M, van der Werff H (2018) Landslide inventory and susceptibility modelling using geospatial tools, in Hunza-Nagar valley, northern Pakistan. *J Mt Sci* 15(6):1354–1370
- Bai SB, Jian W, Guo-Nian L, Zhou PG, Hou SS, Su-Ning XU (2009) GIS-based and data-driven bivariate landslide-susceptibility mapping in the Three Gorges area, China. *Pedosphere* 19(1):14–20
- Bai SB, Wang J, Lü GN, Zhou PG, Hou SS, Xu SN (2010) GIS-based logistic regression for landslide susceptibility mapping of the Zhongxian segment in the Three Gorges area, China. *Geomorphology* 115(1):23–31
- Barella CF, Sobreira FG, Zêzere JL (2019) A comparative analysis of statistical landslide susceptibility mapping in the southeast region of Minas Gerais state, Brazil. *Bull Eng Geol Environ* 78(5):3205–3221
- Binh TP, Prakash I (2019) Evaluation and comparison of LogitBoost ensemble, Fisher's linear discriminant analysis, logistic regression and support vector machines methods for landslide susceptibility mapping. *Geocarto International* 34(3):316–333
- Binh TP, Prakash I, Singh SK, Shirzadi A, Shahabi H, Thi-Thu-Trang T, Dieu TB (2019) Landslide susceptibility modeling using reduced error pruning trees and different ensemble techniques: hybrid machine learning approaches. *Catena* 175:203–218
- Blaschke T, Strobl J (2015) What's wrong with pixels? Some recent developments interfacing remote sensing and GIS. *ISPRS Int J Geo-Inf* 4(12):1–17
- Brabb EE (1987) Innovative approaches to landslide hazard and risk mapping. *Jpn Landslide Soc*:17–22
- Breiman L (2001) Random forests. *Mach Learn* 45(1):5–32
- Bui DT, Tuan TA, Klempe H, Pradhan B, Revhaug I (2016) Spatial prediction models for shallow landslide hazards: a comparative assessment of the efficacy of support vector machines, artificial neural networks, kernel logistic regression, and logistic model tree. *Landslides* 13(2):361–378
- Cama M, Conoscenti C, Lombardo L, Rotigliano E (2016) Exploring relationships between grid cell size and accuracy for debris-flow susceptibility models: a test in the Giampilieri catchment (Sicily, Italy). *Environ Earth Sci* 75(3):238
- Cao J, Cao M, Wang J, Yin C, Wang D, Vidal P (2019a) Urban noise recognition with convolutional neural network. *Multimed Tools Appl* 78(20):29021–29041
- Cao J, Zhang Z, Wang C, Liu J, Zhang L (2019b) Susceptibility assessment of landslides triggered by earthquakes in the Western Sichuan Plateau. *Catena* 175:63–76
- Cascini L (2008) Applicability of landslide susceptibility and hazard zoning at different scales. *Eng Geol* 102(3):164–177
- Chapelle O, Haffner P, Vapnik VN (1999) Support vector machines for histogram-based image classification. *IEEE Trans Neural Netw* 10(5):1055–1064
- Chauhan S, Sharma M, Arora MK (2010) Landslide susceptibility zonation of the Chamoli region, Garhwal Himalayas, using logistic regression model. *Landslides* 7(4):411–423
- Chen W, Li X, Wang Y, Chen G, Liu S (2014) Forested landslide detection using LiDAR data and the random forest algorithm: a case study of the Three Gorges, China. *Remote Sens Environ* 152:291–301
- Cui X, Goel V, Kingsbury B (2014) Data augmentation for deep neural network acoustic modeling. *IEEE Int Conf Acoust* 23(9):1469–1477
- Dieu TB, Shirzadi A, Shahabi H, Geertsema M, Omidvar E, Clague JJ, Binh TP, Dou J, Asl DT, Bin Ahmad B, Lee S (2019) New ensemble models for shallow landslide susceptibility modeling in a semi-arid watershed. *Forests* 10(9):743
- Dong VD, Jaafari A, Bayat M, Mafi-Gholami D, Qi C, Moayedi H, Tran VP, Hai-Bang L, Tien-Thinh L, Phan TT, Chinh L, Nguyen KQ, Bui NT, Binh TP (2020) A spatially explicit deep learning neural network model for the prediction of landslide susceptibility. *Catena* 188:104451
- Dou J, Yunus AP, Dieu TB, Merghadi A, Sahana M, Zhu Z, Chen C, Han Z, Binh TP (2020) Improved landslide assessment using support vector machine with bagging, boosting, and stacking ensemble machine learning framework in a mountainous watershed. *Landslides* 17(3):641–658
- Drăguț L, Blaschke T (2006) Automated classification of landform elements using object-based image analysis. *Geomorphology* 81(3):330–344
- Duo Z, Wang W, Wang H (2019) Oceanic mesoscale eddy detection method based on deep learning. *Remote Sens* 11(16):1921
- Dymond JR, Derose RC, Harmsworth GR (1995) Automated mapping of land components from digital elevation data. *Earth Surf Process Landf* 20(2):131–137
- Ehret D, Rohn J, Dumperth C, Eckstein S, Ernstberger S, Otte K, Rudolph R, Wiedenmann J, Wei X, Bi R (2010) Frequency ratio analysis of mass movements

- in the Xiangxi catchment, Three Gorges Reservoir area, China. *J Earth Sci* 21(6):824–834
- Fang Z, Wang Y, Peng L, Hong H (2020) Integration of convolutional neural network and conventional machine learning classifiers for landslide susceptibility mapping. *Comput Geosci* 104470
- Fell R, Corominas J, Bonnard C, Cascini L, Leroi E, Savage WZ (2007) Guidelines for landslide susceptibility, hazard and risk zoning for land use planning. *Eng Geol* 102(3):85–98
- Gaudio VD, Wasowski J, Muscillo S (2013) New developments in ambient noise analysis to characterise the seismic response of landslide prone slopes. *Nat Hazards Earth Syst Sci* 13(8):2075–2087
- Giles PT, Franklin SE (1998) An automated approach to the classification of the slope units using digital data. *Geomorphology* 21(3):251–264
- Gorsevski PV, Gessler PE, Boll J, Elliot WJ, Foltz RB (2006) Spatially and temporally distributed modeling of landslide susceptibility. *Geomorphology* 80(3–4):178–198. <https://doi.org/10.1016/j.geomorph.2006.02.011>
- Gorsevski PV, Brown MK, Panter K, Onasch CM, Simic A, Snyder J (2016) Landslide detection and susceptibility mapping using LiDAR and an artificial neural network approach: a case study in the Cuyahoga Valley National Park, Ohio. *Landslides* 13(3):467–484
- Gupta SK, Shukla DP, Thakur M (2018) Selection of weightages for causative factors used in preparation of landslide susceptibility zonation (LSZ). *Geomatics Nat Hazards Risk* 9(1):471–487
- Guzzetti F, Carrara A, Cardinali M, Reichenbach P (1999) Landslide hazard evaluation: a review of current techniques and their application in a multi-scale study, Central Italy. *Geomorphology* 31(1):181–216
- Guzzetti F, Reichenbach P, Ardizzone F, Cardinali M, Galli M (2006) Estimating the quality of landslide susceptibility models. *Geomorphology* 81(1):166–184
- Guzzetti F, Mondini AC, Cardinali M, Fiorucci F, Santangelo M, Chang KT (2012) Landslide inventory maps: new tools for an old problem. *Earth Sci Rev* 112(1):42–66
- Hassani H, Ghazanfari M (2008) Landslide susceptibility zonation of the Qazvin-Rasht-Anzali railway track, North Iran. *Int Symp Landslides Eng Slopes*:1911–1917
- Havaei M, Davy A, Wardefarley D, Biard A, Courville A, Bengio Y, Pal C, Jodoin PM, Larochelle H (2017) Brain tumor segmentation with deep neural networks. *Med Image Anal* 35:18–31
- He S, Pan P, Dai L, Wang H, Liu J (2012) Application of kernel-based Fisher discriminant analysis to map landslide susceptibility in the Qinggan River delta, Three Gorges, China. *Geomorphology* 171:30–41
- He K, Zhang X, Ren S, Sun J (2015) Deep residual learning for image recognition. *IEEE Comput Soc* 1:770–778
- He J, Zhuang F, Liu Y, He Q, Lin F (2018) Bayesian dual neural networks for recommendation. *Front Comput Sci* 13(6):1255–1265
- He X, Luo J, Zuo G, Xie J (2019) Daily runoff forecasting using a hybrid model based on variational mode decomposition and deep neural networks. *Water Resour Manag* 33(4):1571–1590
- Hinton G, Deng L, Yu D, Dahl GE, Mohamed A, Jaitly N, Senior A, Vanhoucke V, Nguyen P, Sainath TN, Kingsbury B (2012) Deep neural networks for acoustic modeling in speech recognition. *IEEE Signal Process Mag* 29(6):82–97
- Hong H, Illia I, Tsangaratos P, Chen W, Xu C (2017) A hybrid fuzzy weight of evidence method in landslide susceptibility analysis on the Wuyuan area, China. *Geomorphology* 290:1–16
- Hongyo R, Egashira Y, Hone TM, Yamaguchi K (2019) Deep neural network-based digital predistorter for Doherty power amplifiers. *IEEE Microw Wirel Components Lett* 29(2):146–148
- Hu Q, Zhou Y, Wang S, Wang F, Wang H (2019) Improving the accuracy of landslide detection in “off-site” area by machine learning model portability comparison: a case study of Jiuzhaigou earthquake, China. *Remote Sens* 11(21):2530
- Huang Y, Zhao L (2018) Review on landslide susceptibility mapping using support vector machines. *Catena* 165:520–529
- Jo YJ, Cho H, Sang YL, Choi G, Kim G, Min HS, Park YK (2018) Quantitative phase imaging and artificial intelligence: a review. *IEEE J Sel Top Quantum Electron* 25(1):6800914
- Kamp U, Growley BJ, Khattak GA, Owen LA (2008) GIS-based landslide susceptibility mapping for the 2005 Kashmir earthquake region. *Geomorphology* 101(4):631–642
- Kanungo DP, Sarkar S, Sharma S (2011) Combining neural network with fuzzy, certainty factor and likelihood ratio concepts for spatial prediction of landslides. *Nat Hazards* 59(3):1491–1512
- Kim Y, Kim HG, Choi HJ (2017) Model regularization of deep neural networks for robust clinical opinions generation from general blood test results. *IEEE Int Conf Mobile Data Manag*:386–391
- Kim J, Lee S, Jung H, Lee S (2018) Landslide susceptibility mapping using random forest and boosted tree models in Pyeong-Chang, Korea. *Geocarto Int* 33(9):1000–1015
- Kumar D, Thakur M, Dubey CS, Shukla DP (2017) Landslide susceptibility mapping & prediction using support vector machine for Mandakini River Basin, Garhwal Himalaya, India. *Geomorphology* 295:115–125
- Lagomarsino D, Tofani V, Segoni S, Catani F, Casagli N (2017) A tool for classification and regression using random forest methodology: applications to landslide susceptibility mapping and soil thickness modeling. *Environ Model Assess* 22(3):201–214
- Lee M, Park I, Lee S (2015) Forecasting and validation of landslide susceptibility using an integration of frequency ratio and neuro-fuzzy models: a case study of Seorak mountain area in Korea. *Environ Earth Sci* 74(1):413–429
- Li L, Lan H, Guo C, Zhang Y, Li Q, Wu Y (2017) A modified frequency ratio method for landslide susceptibility assessment. *Landslides* 14(2):727–741
- Liang G, Hui D, Wu X, Wu J, Liu J, Zhou G, Zhang D (2016) Effects of simulated acid rain on soil respiration and its components in a subtropical mixed conifer and broadleaf forest in southern China. *Environ Sci Process Impacts* 18(2):246–255
- Ling P, Niu R, Bo H, Wu X, Zhao Y, Ye R (2014) Landslide susceptibility mapping based on rough set theory and support vector machines: a case of the Three Gorges area, China. *Geomorphology* 204(1):287–301
- Liu Y, Cheng H, Kong X, Wang Q, Cui H (2019) Intelligent wind turbine blade icing detection using supervisory control and data acquisition data and ensemble deep learning. *Energy Sci Eng* 7(6):2633–2645
- Malsburg CVD (1986) Frank Rosenblatt: principles of neurodynamics: perceptrons and the theory of brain mechanisms. *Brain Theory*:245–248
- Mandal SP, Chakrabarty A, Maity P (2018) Comparative evaluation of information value and frequency ratio in landslide susceptibility analysis along national highways of Sikkim Himalaya. *Spat Inf Res* 26(2):127–141
- Martinović K, Gavin K, Reale C (2016) Development of a landslide susceptibility assessment for a rail network. *Eng Geol* 215:1–9
- Meier U, Masci J (2012) Multi-column deep neural network for traffic sign classification. *Neural Netw* 32(1):333–338
- MGMR, Ministry of Geology and Mineral Resources (1988) Study on the bank stability in the Three Gorges engineering in Yangze River. Geological Publishing House, Beijing
- Miao H, Wang G, Yin K, Toshitaka K, Yuanhao LI (2014) Mechanism of the slow-moving landslides in Jurassic red-strata in the Three Gorges Reservoir, China. *Eng Geol* 171(8):59–69
- Mondal S, Mandal S (2019) Landslide susceptibility mapping of Darjeeling Himalaya, India using index of entropy (IOE) model. *Applied Geomatics* 11(2):129–146
- Montrasio L, Schilirò L, Terrone A (2015) Physical and numerical modelling of shallow landslides. *Landslides* 13(5):873–883
- Nefeslioglu HA, Gorum T (2020) The use of landslide hazard maps to determine mitigation priorities in a dam reservoir and its protection area. *Land Use Policy* 91:104363
- Niu R, Wu X, Yao D, Ling P, Li A, Peng J (2017) Susceptibility assessment of landslides triggered by the Lushan earthquake, April 20, 2013, China. *IEEE J Sel Top Appl Earth Observ Remote Sens* 7(9):3979–3992
- Owen LA, Kamp U, Khattak GA, Harp EL, Keefer DK, Bauer MA (2008) Landslides triggered by the 8 October 2005 Kashmir earthquake. *Geomorphology* 94(1):1–9
- Oysal Y (2005) A comparative study of adaptive load frequency controller designs in a power system with dynamic neural network models. *Energy Convers Manag* 46(15–16):2656–2668
- Pamela SJA, Yukni A (2017) Weights of evidence method for landslide susceptibility mapping in Takengon, Central Aceh, Indonesia. *IOP Conf Ser Earth Environ Sci* 118:012037
- Paolo P, Elia R, Bolla A (2013) Influence of filling–drawdown cycles of the Vajont reservoir on Mt. Toc slope stability. *Geomorphology* 191(5):75–93
- Pham BT, Prakash I, Chen W, Ly H, Ho LS, Omidvar E, Tran VP, Tien Bui D (2019) A novel intelligence approach of a sequential minimal optimization-based support vector machine for landslide susceptibility mapping. *Sustainability* 11(22):6323
- Polykretis C, Chalkias C (2018) Comparison and evaluation of landslide susceptibility maps obtained from weight of evidence, logistic regression, and artificial neural network models. *Nat Hazards* 93(1):249–274
- Ramachandra TV, Aithal BH, Kumar U, Joshi NV (2013) Prediction of shallow landslide prone regions in undulating terrains. *Disaster Adv* 6(1):54–64
- Romstad B, Etzelmüller B (2009) Structuring the digital elevation model into landform elements through watershed segmentation of curvature. *Geomorphometry*. University of Zurich, Zürich, pp 55–60
- Romstad B, Etzelmüller B (2012) Mean-curvature watersheds: a simple method for segmentation of a digital elevation model into terrain units. *Geomorphology* 139(2):293–302

- Ronoud S, Asadi S (2019) An evolutionary deep belief network extreme learning-based for breast cancer diagnosis. *Soft Comput* 23(24):13139–13159
- Rowbotham DN, Dudycha D (1998) GIS modelling of slope stability in Phewa Tal watershed, Nepal. *Geomorphology* 26(1):151–170
- Ruette J, Lehmann P, Or D (2013) Rainfall-triggered shallow landslides at catchment scale: threshold mechanics-based modeling for abruptness and localization. *Water Resour Res* 49(10):6266–6285
- Saha AK, Gupta RP, Sarkar I, Arora MK, Csaplovics E (2005) An approach for GIS-based statistical landslide susceptibility zonation—with a case study in the Himalayas. *Landslides* 2(1):61–69
- Seide F, Gang L, Dong Y (2012) Conversational speech transcription using context-dependent deep neural networks. *Int Conference Int Conf Mach Learn* 1-5:444
- Sevgen E, Kocaman S, Nefeslioglu HA, Gokceoglu C (2019) A novel performance assessment approach using photogrammetric techniques for landslide susceptibility mapping with logistic regression, ANN and random forest. *Sensors* 19(18):3940
- Sharif K, Roslee R, Ern LK, Simon N (2017) Landslide factors and susceptibility mapping on natural and artificial slopes in Kundasang, Sabah. *Sains Malaysiana* 46(9):1531–1540
- Shi G, Zhang J, Li H, Wang C (2019) Enhance the performance of deep neural networks via L2 regularization on the input of activations. *Neural Process Lett* 50(1):57–75
- Shirvani Z (2020) A holistic analysis for landslide susceptibility mapping applying geographic object-based random forest: a comparison between protected and non-protected forests. *Remote Sens* 12(3):434
- Stumpf A, Kerle N (2011) Object-oriented mapping of landslides using random forests. *Remote Sens Environ* 115(10):2564–2577
- Tanyas H, Rossi M, Alvioli M, van Westen CJ, Marchesini I (2019) A global slope unit-based method for the near real-time prediction of earthquake-induced landslides. *Geomorphology* 327:126–146
- TGWC, Three Gorges Reservoir Area Geological Disaster Prevention and Control Work Command (2010). Prevention and control of geological disasters in the Three Gorges reservoir area
- Thomas MA, Mirus BB, Collins BD, Ning L, Godt JW (2018) Variability in soil-water retention properties and implications for physics-based simulation of landslide early warning criteria. *Landslides* 15(7):1265–1277
- Torizin J, Wang L, Fuchs M, Tong B, Balzer D, Wan L, Kuhn D, Li A, Chen L (2018) Statistical landslide susceptibility assessment in a dynamic environment: a case study for Lanzhou City, Gansu Province, NW China. *J Mt Sci* 15(6):1299–1318
- Toshev A, Szegedy C (2013) DeepPose: human pose estimation via deep neural networks. *IEEE Conf Comput Vision Pattern Recog*:1653–1660
- van Westen CJ, Castellanos E, Kuriakose SL (2008) Spatial data for landslide susceptibility, hazard, and vulnerability assessment: an overview. *Eng Geol* 102(3):112–131
- Wang L, Guo M, Sawada K, Lin J, Zhang J (2016a) A comparative study of landslide susceptibility maps using logistic regression, frequency ratio, decision tree, weights of evidence and artificial neural network. *Geosci J* 20(1):117–136
- Wang Q, Li W, Wu Y, Pei Y, Xie P (2016b) Application of statistical index and index of entropy methods to landslide susceptibility assessment in Gongliu (Xinjiang, China). *Environ Earth Sci* 75(7):599
- Wang Y, Fang Z, Hong H (2019a) Comparison of convolutional neural networks for landslide susceptibility mapping in Yanshan County, China. *Sci Total Environ* 666:975–993
- Wang Y, Wu X, Chen Z, Ren F, Feng L, Du Q (2019b) Optimizing the predictive ability of machine learning methods for landslide susceptibility mapping using SMOTE for Lishui City in Zhejiang Province, China. *Int J Environ Res Public Health* 16(3):3683
- Wang G, Chen X, Chen W (2020a) Spatial prediction of landslide susceptibility based on GIS and discriminant functions. *ISPRS Int J Geo Inf* 9(3):144
- Wang Y, Fang Z, Wang M, Peng L, Hong H (2020b) Comparative study of landslide susceptibility mapping with different recurrent neural networks. *Comput Geosci* 138:104445
- Wei C, Pourghasemi HR, Zhou Z (2017) A GIS-based comparative study of Dempster-Shafer, logistic regression and artificial neural network models for landslide susceptibility mapping. *Geocarto Int* 32(4):367–385
- Wu X, Niu R, Peng L, Ren F (2013) Landslide susceptibility mapping using rough sets and back-propagation neural networks in the Three Gorges, China. *Environ Earth Sci* 70(3):1307–1318
- Wu X, Fu R, Niu R (2014) Landslide susceptibility assessment using object mapping units, decision tree, and support vector machine models in the Three Gorges of China. *Environ Earth Sci* 71(11):4725–4738
- Wu Y, Bai H, Guo Q, Li W (2016) GIS-based landslide susceptibility analysis using support vector machine model at a regional scale. *Electron J Geotech Eng* 21(14):4427–4434
- Xie M, Esaki T, Zhou G, Mitani Y (2003) Geographic information systems-based three-dimensional critical slope stability analysis and landslide hazard assessment. *J Geotech Geoenviron Eng* 129(12):1109–1118
- Xing H, Zhang G, Shang M (2016) Deep learning. *Int J Semant Comput* 10(3):417–439
- Xu Y, Du J, Dai LR, Lee CH (2015) A regression approach to speech enhancement based on deep neural networks. *IEEE-ACM Trans Audio Speech Lang Process* 23(1):7–19
- Yang SR (2017) Assessment of rainfall-induced landslide susceptibility using GIS-based slope unit approach. *J Perform Constr Facil* 31(4):04017026
- Young T, Palta M, Dempsey J, Skatrud J, Weber S, Badr S (1993) The occurrence of sleep-disordered breathing among middle-aged adults. *N Engl J Med* 328(17):1230–1235
- Youssef AM, Al-Kathery M, Pradhan B (2014) Landslide susceptibility mapping at Al-Hasher Area, Jizan (Saudi Arabia) using GIS-based frequency ratio and index of entropy models. *Geosci J* 19(1):113–134
- Yu L, Cao Y, Zhou C, Wang Y, Huo Z (2019) Landslide susceptibility mapping combining information gain ratio and support vector machines: a case study from Wushan segment in the Three Gorges Reservoir area, China. *Appl Sci Basel* 9(22):4756
- Zêzere JL, Pereira S, Melo R, Oliveira SC, Garcia RA (2017) Mapping landslide susceptibility using data-driven methods. *Sci Total Environ* 589:250–267
- Zhang K, Wu X, Niu R, Yang K, Zhao L (2017) The assessment of landslide susceptibility mapping using random forest and decision tree methods in the Three Gorges Reservoir area, China. *Environ Earth Sci* 76(11):405
- Zhao X, Chen W (2020) GIS-based evaluation of landslide susceptibility models using certainty factors and functional trees-based ensemble techniques. *Appl Sci Basel* 10(1):16
- Zhe L, Yang D, Yang H, Jian Z, Qi Y (2013) Characterizing spatiotemporal variations of hourly rainfall by gauge and radar in the mountainous Three Gorges region. *J Appl Meteorol Climatol* 53(4):873–889
- Zhou C, Shao W, Westen V, Cees J (2014) Comparing two methods to estimate lateral force acting on stabilizing piles for a landslide in the Three Gorges Reservoir, China. *Eng Geol* 173(6):41–53
- Zhu A, Miao Y, Liu J, Bai S, Zeng C, Ma T, Hong H (2019) A similarity-based approach to sampling absence data for landslide susceptibility mapping using data-driven methods. *Catena* 183:104188

Electronic supplementary material The online version of this article (<https://doi.org/10.1007/s10346-020-01444-0>) contains supplementary material, which is available to authorized users.

Y. Hua · X. Wang (✉) · Y. Li · W. Xia

Hubei Subsurface Multi-scale Imaging Key Laboratory, Institute of Geophysics and Geomatics,
China University of Geosciences,
Wuhan, 430074, China
Email: xianminwang@163.com

P. Xu

School of Geography and Information Engineering,
China University of Geosciences,
Wuhan, 430074, China